

An accurate and practical method for inference of weak gravitational lensing from galaxy images

Gary M. Bernstein

`garyb@physics.upenn.edu`

Robert Armstrong¹

`rearmstr@gmail.com`

Christina Krawiec

`ckrawiec@sas.upenn.edu`

and

Marisa C. March

`mamarch@sas.upenn.edu`

Department of Physics & Astronomy, University of Pennsylvania, 209 S. 33rd St., Philadelphia, PA 19104

ABSTRACT

We demonstrate highly accurate recovery of weak gravitational lensing shear using an implementation of the Bayesian Fourier Domain (BFD) method proposed by Bernstein & Armstrong (2014, BA14), extended to correct for selection biases. The BFD formalism is rigorously correct for Nyquist-sampled, background-limited, uncrowded image of background galaxies. BFD does not assign shapes to galaxies, instead compressing the pixel data \mathbf{D} into a vector of moments \mathbf{M} , such that we have an analytic expression for the probability $P(\mathbf{M}|\mathbf{g})$ of obtaining the observations with gravitational lensing distortion \mathbf{g} along the line of sight. We implement an algorithm for conducting BFD's integrations over the population of unlensed source galaxies which measures ≈ 10 galaxies/second/core with good scaling properties. Initial tests of this code on $\approx 10^9$ simulated lensed galaxy images recover the simulated shear to a fractional accuracy of $m = (2.1 \pm 0.4) \times 10^{-3}$, substantially more accurate than has been demonstrated

¹Department of Astrophysical Sciences, Princeton University, Princeton, NJ 08544

previously for any generally applicable method. Deep sky exposures generate a sufficiently accurate approximation to the noiseless, unlensed galaxy population distribution assumed as input to BFD. Potential extensions of the method include simultaneous measurement of magnification and shear; multiple-exposure, multi-band observations; and joint inference of photometric redshifts and lensing tomography.

Subject headings: gravitational lensing: weak—methods: data analysis

1. Introduction

Weak gravitational lensing (WL) provides an unambiguous measurement of the second (and potentially higher) derivatives of the scalar gravitational potential along the line of sight. This has made WL a critical observational window into the behavior and history of the components of the Universe that source the gravitational potential but do not absorb or emit photons. WL can in addition test the laws of gravitation relating the potential to the matter. Several visible/near-IR surveys of thousands of square degrees of sky are now underway, with measurement of WL signals from images of $O(10^8)$ galaxy images as a primary goal: the *Dark Energy Survey (DES)* (Jarvis et al. 2015), the *Kilo-Degree Survey (KiDS)* (Kuijken et al. 2015), and the *Hypersuprime-cam Survey (HSC)* (Takada 2010). Even more ambitious visible/near-IR WL surveys are planned to measure $> 10^9$ galaxy images in the 2020’s: the *Large Synoptic Survey Telescope (LSST)*,¹ the *Euclid* spacecraft (Laureijs et al. 2011),² and the *Wide-Field Infrared Survey Telescope (WFIRST)*.³ WL distortions have also been detected in radio images of galaxies (Chang et al. 2004; Demetroullas & Brown 2015) and of the cosmic microwave background radiation (van Engelen et al. 2012; Das et al. 2014; Planck Collaboration 2015; Giannantonio et al. 2015).

WL signals are known to be difficult to extract from sky images. Along nearly all lines of sight, the dominant manifestations of lensing are a magnification μ and a shear (g_1, g_2) of the image that define a local rotation-free linear transformation of the sky image. In this paper we will concentrate on estimating these parameters from real-space images of galaxies (with some mention of interferometric imaging in Section 6.1). The difficulties include: the signal is weak, with magnification and shear having RMS amplitudes of ≈ 0.02 on cosmological lines of sight; the source galaxies are typically of comparable intrinsic size to the point spread function (PSF) of the imaging, and the PSF has asymmetries and variation larger than the lensing signal; the WL information is primarily in galaxies with modest signal-to-noise ratios ($S/N \lesssim 25$); and the light distribution from galaxies, unlike the CMB, is not described by any known statistical process.

¹<http://www.lsst.org>

²<http://www.euclid-ec.org>

³<http://wfirst.gsfc.nasa.gov>

A series of community-wide blind “challenges” in extracting shear distortion applied to simulated sky images provides a good summary of progress in overcome these obstacles, most recently the GREAT3 challenge (Mandelbaum et al. 2015). A common quantification of the accuracy of inference is to compare a measured shear component g_{meas} to the value g_{true} inserted into the simulation by

$$g_{\text{meas}} - g_{\text{true}} = m g_{\text{true}} + c, \quad (1)$$

where m is the multiplicative or calibration error on the shear, and c is spurious signal uncorrelated with the input shear, *e.g.* due to leakage of PSF asymmetries into g_{meas} . The ambitious next-generation surveys require $|m| \lesssim 10^{-3}$ and $c_{\text{RMS}} \lesssim 10^{-3.5}$ in order to keep shear-measurement errors from degrading the accuracy of cosmological inferences (Huterer et al. 2006; Amara & Réfrégier 2008). The GREAT3 simulated galaxy samples are large enough to measure m to ± 0.003 and c to $\pm 10^{-4}$ at 68% confidence. Over 1000 measurements were submitted to GREAT3 using ≈ 20 distinct methodologies. None were consistently able to achieve $m = c = 0$ at this level of accuracy, though the sFIT algorithm (see Mandelbaum et al. 2015) did so in more than one branch of the challenge. There has not to date been any demonstration of a practical shear inference method that is accurate at the part-per-thousand level we will soon want. In this paper we show that the Bayesian Fourier Domain (BFD) method proposed by Bernstein & Armstrong (2014, BA14) is in this regime, validating the method on simulations similar to some branches of GREAT3. Our validation tests are more demanding than GREAT3 in the sense that we include lower- S/N source images and hence require some correction for selection biases.⁴

Most of the current effort on shear measurement is directed towards model-fitting methods, whereby a parametric model of each galaxy’s appearance is convolved with the PSF and compared to the pixel data. The models are usually concentric combinations of exponential and deVaucouleurs ellipsoids (or other Sérsic profiles). Galaxies are assigned the ellipticity of the model which has the maximum likelihood of reproducing the pixel data, or an ellipticity is assigned from some weighting of the likelihood surface. Model-fitting methods can of course accrue biases because real galaxies are not fully described by the model (Voigt & Bridle 2010; Bernstein 2010). Other methods (*e.g.* Kaiser et al. 1995; Bernstein & Jarvis 2002; Bernstein 2010) assign an ellipticity via model-independent means, typically as some combination of weighted central moments. In both approaches, a shear estimator g_{meas} is produced from some weighted sum of the galaxy ellipticities. While these methods overcome many of the WL inference difficulties noted above, none includes a rigorous treatment of the propagation of image noise through the measurement, and hence incur “noise biases,” *e.g.* because the maximum-likelihood parameters respond asymmetrically to noise, hence can accrue bias in the presence of noise. Furthermore all these methods are subject to selection biases, as the criteria for inclusion and/or weighting of galaxies’ ellipticities implicitly favor certain pre-lensing orientations of the sources. Recovery of unbiased WL estimators then

⁴We have not applied BFD to the public GREAT3 challenge data. The underlying galaxy population for the GREAT3 images was chosen to depend on the observing conditions, hence violating BFD’s basic assumption that deep images are sampling the same population as the target images.

relies upon applying corrections derived empirically from application of the method to simulated images with known lensing distortion (*e.g.* Gruen et al. 2010; Kacprzak et al. 2012). The accuracy of such corrections thus depends upon the simulated images capturing all salient characteristics of the real sky and the observing process.

The largest recent WL cosmology surveys have adopted variants of model-fitting. The *CFHTLS* and *KiDS* surveys use the LENSFIT code, with empirical corrections averaging $m \approx 0.05$ but as large as $m \approx 0.20$ applied as described in Miller et al. (2013). The *DES* Science Verification WL results (Jarvis et al. 2015) use two parallel codes: NGMIX (Sheldon 2014) and IM3SHAPE (Zuntz et al. 2013), the latter with empirical corrections for noise and selection bias which again range up to ≈ 0.2 . Jarvis et al. (2015) conclude from a battery of internal tests and inter-comparisons of the methods that an uncertainty of ± 0.05 should be assigned to m in the final shear catalog. This accuracy is shown to be sufficient for the preliminary results from *DES*, but this and other surveys in progress will soon require WL inferences with $\approx 10\times$ better accuracy. Further, it is disconcerting that the simulation-derived corrections are $\approx 50\times$ larger than the accuracy needed for next-generation WL projects.

BA14 propose a different approach to shear inference. They suggest skipping the estimation of galaxy shape properties, instead evaluating from the outset the probability $P(\mathbf{D}_i|\mathbf{g})$ that the pixel data \mathbf{D}_i from galaxy i would be produced for lensing \mathbf{g} on its line of sight. While a single galaxy provides only weak discrimination on the shear in that the derivative $\nabla_{\mathbf{g}}P$ is small, a large population of sources can tightly constrain the mean \mathbf{g} , or any model for spatially varying WL. The BA14 method relies upon having high- S/N observations of a representative sample of source galaxies, which can be obtained from observations of a subset of the survey region with longer integration times. In other words the model for the unlensed population of target galaxies is that it is drawn from the finite number of galaxies observed in these deep-integration fields—or more specifically, that the targets’ *moments* are drawn from those of the deep-field galaxies, up to rotation and parity transformations (as explained below).

In Section 2 we re-derive the BA14 BFD method, extending the method to include a prescription for detection and selection of sources for which selection biases can be calculated to high accuracy. Section 3 describes our computational implementation of the BFD method, and in Section 4 we demonstrate using simulations similar to GREAT3 that our implementation does indeed recover input shear near part-per-thousand accuracy, potentially unlocking the full power of current and future lensing surveys.

In Section 5 we take inventory of the assumptions and approximations made in deriving the BFD estimators, and assess the extent to which violations of these in real data might compromise the measurement accuracy. We find no show-stoppers yet. In Section 6 we sketch a number of straightforward extensions of the current BFD implementation that will extend its science reach, *e.g.* to measurements of magnification as well as shear, to multi-band or interferometric measurements, and to integrating photometric redshift and tomographic WL inference into a single measurement

process.

2. Formalism

Our goal is to infer the lensing distortion \mathbf{g} from the observational data vector \mathbf{D} . Our current implementation assumes pure-shear distortions, so $\mathbf{g} = (g_1, g_2)$, but the formalism is unchanged if we include magnification μ in \mathbf{g} as well. By Bayes’ theorem

$$P(\mathbf{g}|\mathbf{D}) = \frac{P(\mathbf{D}|\mathbf{g})P(\mathbf{g})}{P(\mathbf{D})}. \quad (2)$$

We will not be concerned with the normalization by the evidence $P(\mathbf{D})$. In this paper we will assume that all galaxies are viewed through a common lensing \mathbf{g} , and that the prior $P(\mathbf{g})$ is much less informative than the data and can be taken as uniform. Thus we focus on determining $P(\mathbf{D}|\mathbf{g})$. We leave to future work the extension of the method to other circumstances, such as when \mathbf{g} is known to follow some parametric form of position (discussed in BA14), or when \mathbf{g} is drawn from a Gaussian random field.

2.1. Simplest case

Ultimately we will need to determine $P(\mathbf{D}|\mathbf{g})$ in the case where the data contain images of an arbitrary number of galaxies at unknown locations. We will assume that the pre-seeing, pre-lensing images are drawn from a known library of “template” galaxies, indexed by G , which in practice we will obtain by observing a fraction of our survey to significantly higher S/N . We begin, however, with a simple case, in which we know we are observing a single galaxy known to have underlying template index G . The position on the sky of some reference point in the galaxy (such as its centroid) we denote as \mathbf{x}_G . Knowing G we simulate the action of the lensing distortions and the observing process (namely the PSF and pixelization) to predict the data vector $\mathbf{D}^G(\mathbf{g}, \mathbf{x}_G)$ that we would obtain from a noiseless observation. The observed data vector is

$$\mathbf{D} = \mathbf{D}^n + \mathbf{D}^G(\mathbf{g}, \mathbf{x}_G), \quad (3)$$

and we assume that we know the likelihood function $\mathcal{L}(\mathbf{D}^n)$ of the added noise. In the case that \mathbf{x}_G is known, we have

$$P(\mathbf{D}|\mathbf{g}) = \mathcal{L}(\mathbf{D}^n) = \mathcal{L}[\mathbf{D} - \mathbf{D}^G(\mathbf{g}, \mathbf{x}_G)]. \quad (4)$$

A central strategy of BFD is to compress the pixel data to a short vector \mathbf{M} that carries most of the information about lensing distortion. The critical requirement on the compression is that we are able to propagate the distribution of \mathbf{D}^n into a probability $P(\mathbf{M}|\mathbf{M}^G)$ of observing compressed data \mathbf{M} given that the noiseless underlying galaxy image compresses to \mathbf{M}^G . This is

most straightforwardly accomplished by having the compression be a linear operation on \mathbf{D} such that Equation (3) becomes

$$\mathbf{M} = \mathbf{M}^n + \mathbf{M}^G(\mathbf{g}, \mathbf{x}_G), \quad (5)$$

and we will have, for fixed \mathbf{x}_G ,

$$P(\mathbf{M}|\mathbf{g}) = \mathcal{L}(\mathbf{M}^n) = \mathcal{L}[\mathbf{M} - \mathbf{M}^G(\mathbf{g}, \mathbf{x}_G)]. \quad (6)$$

We choose for \mathbf{M} a set of moments of the Fourier transform $\tilde{I}^o(\mathbf{k})$ of the observed surface brightness $I^o(\mathbf{x})$, defined as

$$\tilde{I}^o(\mathbf{k}; \mathbf{x}_0) \equiv \int d^2x I^o(\mathbf{x}) e^{-i\mathbf{k} \cdot (\mathbf{x} - \mathbf{x}_0)} \quad (7)$$

Note that this compression requires a choice \mathbf{x}_0 of coordinate origin. In this section we will assume that we have *a priori* knowledge of \mathbf{x}_G and can set $\mathbf{x}_0 = \mathbf{x}_G$. In the next section we will develop a treatment for the case of unknown \mathbf{x}_G . The data \mathbf{D} are a regular sampling of I^o , so in practice the Fourier transforms are discrete. We choose the compressed data vector

$$\mathbf{M}(\mathbf{x}_0) \equiv \begin{pmatrix} M_f \\ M_r \\ M_+ \\ M_\times \end{pmatrix} = \int d^2k \frac{\tilde{I}^o(\mathbf{k}; \mathbf{x}_0)}{\tilde{T}(\mathbf{k})} W(|\mathbf{k}^2|) \mathbf{F}; \quad \mathbf{F} \equiv \begin{pmatrix} 1 \\ k_x^2 + k_y^2 \\ k_x^2 - k_y^2 \\ 2k_x k_y \end{pmatrix}. \quad (8)$$

where $\tilde{T}(\mathbf{k})$ is the Fourier transform of the PSF that has convolved the observed image. $W(|\mathbf{k}^2|)$ is a real-valued window function applied to the integral to bound the noise, in particular confining the integral to the finite region of \mathbf{k} in which $\tilde{T}(\mathbf{k})$ is non-zero. We calculate the moments in Fourier domain in order to simplify the removal of the effects of the PSF, but these moments are equivalent to taking radially weighted zeroth and second moments of the real-space, pre-seeing image of the galaxy.

The moments are *not* normalized, so that \mathbf{M} remains a linear function of \mathbf{D} . The noise moment vector, being a sum over the statistically independent noise of many pixels, will have a likelihood $\mathcal{L}(\mathbf{M}^n)$ rapidly tend toward a multivariate Gaussian with covariance matrix \mathbf{C}_M . We assume that *the pixel noise \mathbf{D}^n is stationary*, in which case there is no covariance between the noise at distinct \mathbf{k} values, and the covariance matrix elements are related to the power spectrum $P_n(\mathbf{k})$ of the noise by

$$(\mathbf{C}_M)_{ij} = \int d^2k P_n(\mathbf{k}) \left| \frac{W(|\mathbf{k}^2|)}{\tilde{T}(\mathbf{k})} \right|^2 F_i(\mathbf{k}) F_j^*(\mathbf{k}). \quad (9)$$

Note that while background shot noise and detector read noise are stationary, any significant shot noise from the galaxy's photons will violate stationarity. With sensible choice of W , the moments \mathbf{M} carry most of the information available about shear of the source (Bernstein & Jarvis 2002). There are many practical benefits to discarding the rest of the information in \mathbf{D} , as will become apparent, but we highlight first that \mathbf{M}^G is independent of the observational conditions, *i.e.* has

been corrected for the PSF, so we do not need to recalculate \mathbf{M}^G as the PSF varies, as long as we hold W fixed.

We note at this point that there is much freedom in the choice of W . As long as W leads to finite noise \mathbf{C}_M via Equation (9), BFD remains valid and unbiased; but the accuracy of the inference on \mathbf{g} will depend upon the choice of W . One may choose to adjust this weight to optimize shear inference for a given set of observing conditions, but it is critical that the choice does *not* depend upon the properties of target galaxies. In this sense the BFD method is sub-optimal, in that it may not extract the most precise measure of \mathbf{g} from both large and small galaxies simultaneously. We describe one choice for W in Section 3.3.

The next assumption in BFD is that *the lensing is weak, so that a second-order Taylor expansion about $\mathbf{g} = 0$ fully describes $P(\mathbf{M}|\mathbf{g})$ for observed values of \mathbf{g}* . In this case we have

$$P(\mathbf{M}|\mathbf{g}) = P + \mathbf{Q} \cdot \mathbf{g} + \frac{1}{2} \mathbf{g} \cdot \mathbf{R} \cdot \mathbf{g}, \quad (10)$$

$$P \equiv P(\mathbf{M}|\mathbf{g} = 0) = \mathcal{L}(\mathbf{M} - \mathbf{M}^G) = |2\pi\mathbf{C}_M|^{-1/2} \exp \left[-(\mathbf{M} - \mathbf{M}^G)^T \mathbf{C}_M^{-1} (\mathbf{M} - \mathbf{M}^G) \right], \quad (11)$$

$$\mathbf{Q} \equiv \nabla_{\mathbf{g}} P(\mathbf{M}|\mathbf{g})|_{\mathbf{g}=0} = -\nabla_{\mathbf{g}} \mathbf{M}^G \cdot \nabla_{\mathbf{M}} \mathcal{L}(\mathbf{M} - \mathbf{M}^G) \quad (12)$$

$$\mathbf{R} \equiv \nabla_{\mathbf{g}} \nabla_{\mathbf{g}} P(\mathbf{M}|\mathbf{g})|_{\mathbf{g}=0}. \quad (13)$$

At the end of Equation (12) we have assumed that *the noise likelihood is invariant under shear of the underlying galaxy G* so that we can propagate all shear derivatives into derivatives of the properties of the template galaxy. This is satisfied for background-limited images. The quantities \mathbf{Q} and \mathbf{R} give the differential probability of observing the image under lensing distortions. If \mathbf{D} is comprised of many independent observations \mathbf{D}_i of the same underlying galaxy G with the same applied lensing, we can produce the quantities $P_i, \mathbf{Q}_i, \mathbf{R}_i$ as above for each observation, then the total posterior probability for \mathbf{g} is given by

$$-\ln P(\mathbf{g}|\mathbf{D}) = (\text{const}) - \ln P(\mathbf{g}) - \sum_i \ln P(\mathbf{D}_i|\mathbf{g}) \quad (14)$$

$$= (\text{const}) - \ln P(\mathbf{g}) - \mathbf{g} \cdot \mathbf{Q}_{\text{tot}} + \frac{1}{2} \mathbf{g} \cdot \mathbf{R}_{\text{tot}} \cdot \mathbf{g}, \quad (15)$$

$$\mathbf{Q}_{\text{tot}} \equiv \sum_i \frac{\mathbf{Q}_i}{P_i} \quad (16)$$

$$\mathbf{R}_{\text{tot}} \equiv \sum_i \left(\frac{\mathbf{Q}_i \mathbf{Q}_i^T}{P_i^2} - \frac{\mathbf{R}_i}{P_i} \right) \quad (17)$$

The posterior distribution is, ignoring the prior, Gaussian in \mathbf{g} , with inverse covariance matrix

$$\mathbf{C}_g = \mathbf{R}_{\text{tot}}^{-1} \quad (18)$$

and mean value

$$\bar{\mathbf{g}} = \mathbf{R}_{\text{tot}}^{-1} \mathbf{Q}_{\text{tot}}. \quad (19)$$

2.2. Detection and selection

Consider now the case where there is a galaxy present but we do not know its position \mathbf{x}_G in advance, so we need a prescription for choosing those locations \mathbf{x}_0 about which we will compute moments. We need a *detection* process to decide if the galaxy has been observed within some small region $\Delta^2 x$ about some position \mathbf{x}_0 . Once a detection is made, we will also require some *selection* criteria to decide which detections will be used to constrain the lensing. In this section, we will continue to assume that the unlensed appearance G of the galaxy is known, but its location is not. At each potential source location, we end up with either a successful detection and selection, plus measured moments \mathbf{M} ; or a non-selection. We therefore need to know $P(\mathbf{M}, s, d|G) = P(\mathbf{M}, s|G)$ for the former case, and $1 - P(s|G)$ for the latter case, where s (d) indicates successful selection (detection).

These probabilities are readily calculable if we make the detection and selection using the compressed quantities themselves. We add to our compressed data set the two weighted first moments of the source in Fourier space:

$$\mathbf{X}(\mathbf{x}_0) \equiv \int d^2 k \frac{\tilde{I}^o(\mathbf{k}; \mathbf{x}_0)}{\tilde{T}(\mathbf{k})} W(|\mathbf{k}^2|) \begin{pmatrix} ik_x \\ ik_y \end{pmatrix}. \quad (20)$$

We choose as a criterion for detection of a source at \mathbf{x}_0 that $\mathbf{X}(\mathbf{x}_0) = 0$. Our choice of moments for \mathbf{M} and \mathbf{X} have these useful properties:

$$\frac{dM_f}{d\mathbf{x}_0} = \mathbf{X}, \quad (21)$$

$$\text{Cov}(\mathbf{M}, \mathbf{X}) = 0 \quad (\text{for stationary noise}), \quad (22)$$

$$J \equiv \left| \frac{d\mathbf{X}}{d\mathbf{x}_0} \right| = (M_r^2 - M_+^2 - M_\times^2) / 4 = \mathbf{M}^T \mathbf{B} \mathbf{M}, \quad (23)$$

$$\mathbf{B} \equiv \text{diag}(0, 1/4, -1/4, -1/4), \quad (24)$$

$$\langle J^n \rangle = \text{Tr}(\mathbf{B} \mathbf{C}_M) = 0, \quad (25)$$

The first line means that we detect a source at all stationary points of the function $f(\mathbf{x}_0) = M_f$, the zeroth moment of the image as convolved with a filter defined by $W(|\mathbf{k}^2|)/\tilde{T}(\mathbf{k})$. This filter will be broader than the PSF in any sensible application of BFD. The second property yields $\mathcal{L}(\mathbf{M}^n, \mathbf{X}^n) = \mathcal{L}(\mathbf{M}^n) \mathcal{L}(\mathbf{X}^n)$ for our multivariate Gaussian noise distribution. The third property shows that the Jacobian determinant J of the positional moments \mathbf{X} is purely a function of \mathbf{M} , and hence statistically independent of \mathbf{X} .

The noiseless moments expected from galaxy G are now functions $\mathbf{D}^G(\mathbf{g}, \mathbf{u} = \mathbf{x}_G - \mathbf{x}_0)$ and $\mathbf{X}^G(\mathbf{g}, \mathbf{u})$ since it is only the displacement \mathbf{u} between the galaxy location and the Fourier phase center that matters. The detection condition is $\mathbf{X} = \mathbf{X}^G + \mathbf{X}^n = 0$ so the probability of this

occurring in a small region $\Delta^2 x$ about \mathbf{x}_0 is

$$P(\mathbf{M}, d|G, \mathbf{g}, \mathbf{x}_G, \mathbf{x}_0) = \mathcal{L}[\mathbf{M} - \mathbf{M}^G(\mathbf{g}, \mathbf{x}_G - \mathbf{x}_0)] \mathcal{L}[-\mathbf{X}^G(\mathbf{g}, \mathbf{x}_G - \mathbf{x}_0)] \left| \frac{d\mathbf{X}}{d\mathbf{x}_0} \right| P(\mathbf{x}_0) \Delta^2 x \quad (26)$$

$$= \mathcal{L}[\mathbf{M} - \mathbf{M}^G(\mathbf{g}, \mathbf{x}_G - \mathbf{x}_0)] \mathcal{L}[\mathbf{X}^G(\mathbf{g}, \mathbf{x}_G - \mathbf{x}_0)] |J| \Delta^2 x. \quad (27)$$

In the last line, we take advantage of (23), assume a uniform prior $P(\mathbf{x}_0)$ on the position of the detection, and note that the zero-mean, multivariate Gaussian will have $\mathcal{L}(-\mathbf{X}^G) = \mathcal{L}(\mathbf{X}^G)$.

To eliminate noise detections, we will want to discard low-flux detections. We implement the selection criterion as membership in a subregion S of moment space:

$$S : f_{\min} < f < f_{\max} \quad (28)$$

$$\Rightarrow P(\mathbf{M}, s|G, \mathbf{g}, \mathbf{x}_G, \mathbf{x}_0) = \begin{cases} \mathcal{L}(\mathbf{M} - \mathbf{M}^G) \mathcal{L}(\mathbf{X}^G) |J| \Delta^2 x & \mathbf{M} \in S \\ 0 & \mathbf{M} \notin S \end{cases} \quad (29)$$

$$\Rightarrow P(s|G, \mathbf{g}, \mathbf{u} = \mathbf{x}_G - \mathbf{x}_0) = \mathcal{L}(\mathbf{X}^G) \Delta^2 x \int_{\mathbf{M} \in S} d\mathbf{M} \mathcal{L}(\mathbf{M} - \mathbf{M}^G) |J(\mathbf{M})|. \quad (30)$$

For brevity we suppress the dependence of the template galaxy's moments $\mathbf{M}^G, \mathbf{X}^G$ on the applied lensing \mathbf{g} and on the displacement $\mathbf{x}_G - \mathbf{x}_0$ between the galaxy position and the detection location.

To render the integration in (30) tractable, we make the simplifying assumption that *the Jacobian determinant J of the first moments is positive at any location where there is non-negligible probability of selection*:

$$J = \mathbf{M}^T \mathbf{B} \mathbf{M} = J^G + 2(\mathbf{M}^G)^T \mathbf{B} \mathbf{M}^n + J^n > 0. \quad (31)$$

Since J is the determinant of the 2nd derivative matrix of f , a restatement is that we are assuming the $f(\mathbf{x}_0)$ surface is (nearly) always convex if $f_{\min} < f < f_{\max}$. To maintain this approximation we will need to avoid noise detections by raising $f_{\min} \gtrsim 5\sigma_f$, where we define

$$\sigma_f^2 = (\mathbf{C}_M)_{ff}. \quad (32)$$

We discuss this convex-detection approximation in Section 5.3. With this approximation, we can integrate a multivariate Gaussian \mathcal{L} in Equation (30) analytically, obtaining

$$P(s|G, \mathbf{g}, \mathbf{u}) = \mathcal{L}(\mathbf{X}^G) \Delta^2 x \left[J^G Y + 2(\mathbf{C}_M \mathbf{B} \mathbf{M}^G)_f \frac{\partial Y}{\partial f_G} + (\mathbf{C}_M \mathbf{B} \mathbf{C}_M)_{ff} \frac{\partial^2 Y}{\partial f_G^2} \right], \quad (33)$$

$$Y \equiv (2\pi)^{-1/2} \int_{(f_{\min} - f_G)/\sigma_f}^{(f_{\max} - f_G)/\sigma_f} d\nu e^{-\nu^2/2}. \quad (34)$$

Now consider the joint distribution of the detection/selection outcomes at a grid $\mathbf{x}_1, \mathbf{x}_2, \dots, \mathbf{x}_j \dots$ of all search positions with non-negligible selection probability $P(s|G, \mathbf{x}_G, \mathbf{x}_0 = \mathbf{x}_j)$. We assume

now that *galaxies are uncrowded, in that no other galaxies contribute significantly to \mathbf{M} or \mathbf{X} at any location \mathbf{x}_j where galaxy G might be selected.* At each search position, we either have a selection and a resultant \mathbf{M} , or we have a non-selection. If the search region is contiguous, there can be *at most one* of the \mathbf{x}_j with successful selection. This follows from our assumption that $J > 0$, which implies that that map $\mathbf{x}_0 \rightarrow \mathbf{X}$ is one-to-one over a contiguous region, so that $\mathbf{X} = 0$ can only occur at a single \mathbf{x}_0 .

With this single-selection rule, we have two possible outcomes:

1. A detection at a single location \mathbf{x}_j yielding moments \mathbf{M} , with probability $P(\mathbf{M}, s_j|G)$ from Equation (29), or
2. No detection at all, with probability $1 - \sum_j P(s_j|G)$, using the selection probability in Equation (33).

Integrating over all possible detection positions, we obtain a total probability of outcome (1):

$$P(\mathbf{M}, s|G, \mathbf{g}, \mathbf{x}_G) = J(\mathbf{M}) \int d^2u \mathcal{L}[\mathbf{X}^G(\mathbf{g}, \mathbf{u})] \mathcal{L}[\mathbf{M} - \mathbf{M}^G(\mathbf{g}, \mathbf{u})]. \quad (35)$$

$$\approx J(\mathbf{M}) \sum_{\mathbf{u}} \Delta^2u \mathcal{L}[\mathbf{X}^G(\mathbf{g}, \mathbf{u})] \mathcal{L}[\mathbf{M} - \mathbf{M}^G(\mathbf{g}, \mathbf{u})]. \quad (36)$$

In the second line, we change the integration to a sum over a 2d grid of points \mathbf{u} with cell area Δ^2u , since this is how we implement the integration over source position. We can truncate the grid where $P(s_j|G)$ becomes negligible. As expected, the resulting probabilities are independent of both the true position \mathbf{x}_G of the galaxy and the position \mathbf{x}_i of the detection once the observed moments \mathbf{M} are specified.

The total probability of detection is obtained by similarly integrating Equation (33) over all \mathbf{u} :

$$P(s|G, \mathbf{g}) = \sum_{\mathbf{u}} \Delta^2u \mathcal{L}(\mathbf{X}^G) \left\{ J(\mathbf{M}^G) Y + 2(\mathbf{C}_M \mathbf{B} \mathbf{M}^G)_f \frac{\partial Y}{\partial f_G} + (\mathbf{C}_M \mathbf{B} \mathbf{C}_M)_{ff} \frac{\partial^2 Y}{\partial f_G^2} \right\}, \quad (37)$$

remembering that $\mathbf{M}^G, \mathbf{X}^G, f_G$, and the arguments to Y depend upon \mathbf{g} and \mathbf{u} . For a galaxy with flux f_G that is many σ_f away from the selection boundaries, we have $Y \rightarrow 1$. In this case it is easy to see that $P(s|G, \mathbf{g}) \rightarrow 1$, by recasting (37) as an integral over \mathbf{X}^G —as long as $J > 0$. If the positive- J assumption does not hold, Equation (37) is incorrect, and we can have a mean number of detections per source that is > 1 . In Section 5.3 we discuss our approach to mitigating failure of the positive- J assumption.

2.3. Galaxy populations: postage stamp case

Now we generalize from having a single galaxy type G to having G be an index into the entire catalog of possible galaxy images. We assume we know the prior probability p_G that a galaxy is

of type G . If for example the galaxy library is approximated by the set of galaxies found in a high- S/N imaging survey of the sky, each detected galaxy would be assigned equal p_G .

First consider the artificial case (commonly used in shear-testing programs) in which we know that exactly one galaxy has been placed in each of many disjoint “postage stamps” of pixels $\mathbf{D}_i \in \mathbf{D}$. In each stamp, we either obtain a selection with measurement of moments \mathbf{M}_i at some location in the stamp, or we obtain a non-selection. The probabilities of these two outcomes are

$$P(\mathbf{M}_i, s|\mathbf{g}) = J(\mathbf{M}_i) \sum_{G, \mathbf{u}} p_G \Delta^2 u \mathcal{L}(\mathbf{X}^G) \mathcal{L}(\mathbf{M}_i - \mathbf{M}^G), \quad (38)$$

$$P(\sim s|\mathbf{g}) = 1 - P(s|\mathbf{g}) \quad (39)$$

$$P(s|\mathbf{g}) = \sum_{G, \mathbf{u}} p_G \Delta^2 u \mathcal{L}(\mathbf{X}^G) \left[J(\mathbf{M}^G) Y + 2(\mathbf{C}_M \mathbf{B} \mathbf{M}^G)_f \frac{\partial Y}{\partial f_G} + (\mathbf{C}_M \mathbf{B} \mathbf{C}_M)_{ff} \frac{\partial^2 Y}{\partial f_G^2} \right] \quad (40)$$

These are the key equations for the BFD calculation. We have made implicit the dependence of the noiseless template moments \mathbf{M}^G and \mathbf{X}^G on the source position \mathbf{u} and the lensing \mathbf{g} . We define as before the Taylor expansions

$$P(\mathbf{M}_i, s|\mathbf{g}) \approx P_i + \mathbf{Q}_i \cdot \mathbf{g} + \frac{1}{2} \mathbf{g} \cdot \mathbf{R}_i \cdot \mathbf{g}, \quad (41)$$

$$P(s|\mathbf{g}) \approx P_s + \mathbf{Q}_s \cdot \mathbf{g} + \frac{1}{2} \mathbf{g} \cdot \mathbf{R}_s \cdot \mathbf{g}, \quad (42)$$

where $\mathbf{Q}_i = \nabla_{\mathbf{g}} P(\mathbf{M}_i, s)$, etc., are derived by propagating derivatives through to template quantities \mathbf{M}^G and \mathbf{X}^G . The detection probability $P(s)$ is integrated over all possible selected moments and all possible galaxies G , so it does not depend on the data in stamp i , only on the noise level and PSF of the observation as manifested in the covariance matrix \mathbf{C}_M in each stamp. For notational simplicity we will assume here that all stamps have the same noise level and PSF and hence the same \mathbf{C}_M , but the formalism and our implementation allow for variation between targets.

The combined probability of the output of the observation/detection/selection/compression process is

$$P(\mathbf{D}|\mathbf{g}) = P(\sim s|\mathbf{g})^{N_{ns}} \prod_{i \in \text{selections}} P(\mathbf{M}_i, s|\mathbf{g}) \quad (43)$$

where N_{ns} is the number of non-selected stamps. We can now calculate the probability of the lensing variables, following Equation (15):

$$-\ln P(\mathbf{g}|\mathbf{D}) = (\text{const}) - \ln P(\mathbf{g}) - \mathbf{g} \cdot \mathbf{Q}_{\text{tot}} + \frac{1}{2} \mathbf{g} \cdot \mathbf{R}_{\text{tot}} \cdot \mathbf{g}, \quad (44)$$

$$\mathbf{Q}_{\text{tot}} \equiv \sum_i \frac{\mathbf{Q}_i}{P_i} - N_{ns} \frac{\mathbf{Q}_s}{1 - P_s} \quad (45)$$

$$\mathbf{R}_{\text{tot}} \equiv \sum_i \left(\frac{\mathbf{Q}_i \mathbf{Q}_i^T}{P_i^2} - \frac{\mathbf{R}_i}{P_i} \right) + N_{ns} \left(\frac{\mathbf{Q}_s \mathbf{Q}_s^T}{(1 - P_s)^2} + \frac{\mathbf{R}_s}{1 - P_s} \right) \quad (46)$$

We now have all the tools needed to make a lensing inference from a postage-stamp data set. We assume that we have available a *complete catalog of possible galaxies* G and that for each we have a *noiseless, unlensed image*. In practice of course our template set will be a finite sample from the (infinite) distribution of detectable galaxies. It is essential that the template set is a fair sample of all galaxy types that can meet the selection criteria with non-negligible probability. In other words we must know about galaxies that are outside the flux selection cuts by up to several σ_f .

The input data are: postage stamps of the “observed” galaxies, which we call the *targets*; low-noise postage stamp images of unlensed *template* galaxies to serve as our sample G ; the PSF for each stamp; and the noise power spectrum P_n for each stamp. Our testing assumes white noise, $P_n = n$.

The procedure is as follows:

1. Select a weight function W that will be applied to all targets and templates. The best choice will usually be a rotationally symmetric approximation to $\tilde{T}(\mathbf{k})^2 \tilde{I}_g(\mathbf{k})$, where \tilde{I}_g is the transform of the unlensed, pre-seeing image of a galaxy of typical size in the survey.
2. For each template galaxy G , measure the moments \mathbf{X}^G and \mathbf{M}^G under W for copies of the galaxy translated over a grid of \mathbf{x}_G centered on the primary flux peak. We can purge from the template set any that have negligible $P(s|G)$. Further calculate the first and second derivatives of all moments with respect to \mathbf{g} , using the formulae in Appendix C.
3. For each target galaxy:
 - (a) Find the point(s) near the object centroid where the detection criterion $\mathbf{X} = 0$ is met.
 - (b) Calculate the moments \mathbf{M}_i about the detection point(s) and discard those failing the selection cut on the flux moment. After this step we require *no further access to the image data*.
 - (c) If no selection is made, increment the count N_{ns} of non-selections, and continue with the next stamp. If more than one selection is made, choose the brightest and note that we have violated one of our assumptions!
 - (d) Calculate \mathbf{C}_M for this stamp.
 - (e) For each target postage stamp i , calculate $P_i = P(\mathbf{M}_i, s|\mathbf{g} = 0)$ from Equation (38), and also the derivatives under lensing \mathbf{Q}_i and \mathbf{R}_i . Since this operation is executed for every target-template pair, it is the computational bottleneck of the procedure. The summand in (38) is simple, involving some 4-dimensional matrix algebra and one exponential, so is far faster than an iteration of a forward-modeling procedure. The $\{P_i, \mathbf{Q}_i, \mathbf{R}_i\}$ data fully encapsulate the lensing information from this galaxy and go into our catalog.
4. Calculate the selection probability $P(s|\mathbf{g} = 0)$ from Equation (40), and its derivatives $\mathbf{Q}_s, \mathbf{R}_s$ with respect to lensing. Note this needs to be done only once for each distinct \mathbf{C}_M .

5. Sum the contributions to the posterior $-\ln P(\mathbf{g}|\mathbf{D})$ from detections and non-detections as given in Equations (45) and (46).
6. Add the Taylor expansion of any prior $P(\mathbf{g})$ to \mathbf{Q}_{tot} and \mathbf{R}_{tot} .
7. We now have the posterior log probability for \mathbf{g} . The shear estimate and its variance are in Equations (19) and (18).

2.4. Poisson-distributed galaxies

For real sky images, we replace the postage-stamp distribution of galaxies with a Poisson distribution. We assume a total unlensed density n of sources on the sky, with probabilities p_G of each galaxy being of type G . If our target survey spans solid angle Ω of sky, consider dividing this area up into regions of area $\Delta\Omega$ larger than the selection region of any single galaxy, but small enough that $n\Delta\Omega \ll 1$ so that we only have 0 or 1 galaxy in the region after running the detection/selection/compression process across the survey. The probability of obtaining a detection with moments \mathbf{M}_i within any small sky area $\Delta\Omega$ is

$$P(\mathbf{M}_i, s|\mathbf{g}, \Delta\Omega) = \sum_G P(\mathbf{M}_i, s|\mathbf{g}, G) P(G|\Delta\Omega) \quad (47)$$

$$= n \Delta\Omega P(\mathbf{M}_i, s|\mathbf{g}), \quad (48)$$

where we take $P(\mathbf{M}_i, s|\mathbf{g})$ from Equation (38). Similarly, the probability of selecting a source in a single cell

$$P(s|\mathbf{g}, \Delta\Omega) = n \Delta\Omega \sum_G p_G P(s|G, \mathbf{g}), \quad (49)$$

$$= n \Delta\Omega P(s|\mathbf{g}), \quad (50)$$

where we use $P(s|\mathbf{g})$ from Equation (40). The quantity $nP(s|\mathbf{g})$ is the expected sky density of selected galaxies. It depends on \mathbf{g} through the moments of the template galaxies, as per usual.

Our total data \mathbf{D} are reduced to a list $\{\mathbf{M}_i, \mathbf{x}_i\}$ for $1 \leq i \leq N_s$ of the locations and moments of the N_s selected sources; plus the information that there are no selections at any other locations. The total posterior for \mathbf{g} is now

$$P(\mathbf{g}|\mathbf{D}) \propto P(\mathbf{g}) \prod_{\text{non-detections}} [1 - P(s|\mathbf{g}, \Delta\Omega)] \prod_{i=1}^{N_s} P(\mathbf{M}_i, s|\mathbf{g}, \Delta\Omega) \quad (51)$$

$$= P(\mathbf{g}) e^{-n\Omega P(s|\mathbf{g})} (n\Delta\Omega)^{N_s} \prod_{i=1}^{N_s} P(\mathbf{M}_i, s|\mathbf{g}). \quad (52)$$

The $(\Delta\Omega)^{N_s}$ term is independent of \mathbf{g} and can be dropped. We retain dependence on n since we may wish to consider the source density as a free parameter along with \mathbf{g} if we are simultaneously

constraining source clustering and shear. This posterior differs from the postage-stamp case only in the non-selection term. We replace (45) and (46) with

$$-\ln P(\mathbf{g}|\mathbf{D}) = (\text{const}) - \ln P(\mathbf{g}) - N_s \log n + n\Omega P_s - \mathbf{g} \cdot \mathbf{Q}_{\text{tot}} + \frac{1}{2} \mathbf{g} \cdot \mathbf{R}_{\text{tot}} \cdot \mathbf{g}, \quad (53)$$

$$\mathbf{Q}_{\text{tot}} \equiv \sum_i \frac{\mathbf{Q}_i}{P_i} - n\Omega \mathbf{Q}_s, \quad (54)$$

$$\mathbf{R}_{\text{tot}} \equiv \sum_i \left(\frac{\mathbf{Q}_i \mathbf{Q}_i^T}{P_i^2} - \frac{\mathbf{R}_i}{P_i} \right) + n\Omega \mathbf{R}_s \quad (55)$$

The operative procedure for inferring shear from a sky image is hence identical to that given for the postage-stamp case, except that of course we search the entire image for detections, not just the centers of each stamp. We use the above formulae in step 5 instead of the postage-stamp formulae.

2.5. Sampling the template space

The BFD method depends upon approximating the full galaxy population with a finite sample of galaxies G from the sky. In essence we are approximating the continuous distribution of galaxies in the moment space with a set of N_G δ functions at a random sampling from the distribution. The measurement error distribution $\mathcal{L}(\mathbf{M} - \mathbf{M}^G)$ acts as a smoothing kernel over the samples. While the sums over G for P_i (and $\mathbf{Q}_i, \mathbf{R}_i$) in Equation (38) are unbiased estimates of the complete integrals over moment space, there are two issues we must address.

First, in producing \mathbf{Q}_{tot} and \mathbf{R}_{tot} we divide \mathbf{Q}_i and \mathbf{R}_i by P_i . As noted in BA14, division by a noisy estimator for P_i produces a bias that scales inversely with the number of template galaxies contributing significantly to the P_i sums. The number of galaxies we can measure at sufficiently high S/N to use as templates will be limited by scarce observing time. Fortunately we can increase the density of templates in moment space by exploiting the rotation and parity symmetry of the unlensed sky: for each G that we observe, we can assume that rotated and reflected copies of this galaxy are also equally likely to exist. In practice we partition p_G among such copies and add them to the template set. We will investigate in Section 5.7 the bias resulting from finite template sampling.

Second: because our \mathbf{M} consists of un-normalized moments, the spacing between template galaxies in moment space will become large compared to the measurement error ellipsoid described by \mathbf{C}_M when we observe target galaxies at high S/N . Bright targets can easily end up with no templates for which $\mathcal{L}(\mathbf{M} - \mathbf{M}^G)$ is non-negligible. Even worse, the P_i sum for a galaxy can be dominated by a single template that is many σ away from the target in moment space, and this produces large derivatives in $\ln P(\mathbf{M}_i, s)$ with respect to \mathbf{g} , giving spuriously large influence in the final lensing estimator. It is further true that brighter galaxies are rarer on the sky, so our template survey will contain fewer sources with flux comparable to our brighter targets.

It is therefore advantageous to *add noise to the moments measured for bright galaxies*. One may question the sanity of adding noise to hard-won signal, but note that weak shear (magnification) measurements accrue uncertainty from the intrinsic variation of galaxy shapes (sizes) as well as from the measurement noise in these quantities. Typically, once $S/N \gtrsim 20$, the intrinsic variation of the population is the dominant form of noise. So a resolved galaxy with $S/N \approx 75$ loses little lensing information if degraded to $S/N \approx 25$. However if we triple the noise, the likelihood function will “touch” $3^4 \times$ more template galaxies in our 4-dimensional \mathbf{M} space, so we can reduce template sample variance and bias by increasing noise.

We must be careful to implement this process such that $P(\mathbf{M}, s|G, \mathbf{g})$ remains calculable for both the bright galaxies and faint ones. Again this is best done by using the moments themselves to decide whether to add additional noise. The procedure that we use is as follows; in Appendix A we present the altered formulae for $P(\mathbf{M}, s|G, \mathbf{g})$ that apply to the galaxies which have had noise added.

1. We establish bounds f_1 and f_2 on the galaxies to which we wish to add noise, based on comparing the density of templates with the covariance matrix \mathbf{C}_M of the measured moments.
2. We detect, measure, and select target galaxies the same way as described in Section 2.3, in the flux range $f_1 < f < f_2$.
3. For each selected galaxy, we form a new moment vector $\mathcal{M} = \mathbf{M} + \mathbf{M}_A$, with \mathbf{M}_A drawn from a multivariate Gaussian with zero mean and predetermined covariance matrix \mathbf{C}_A . We make no further use of the original moments \mathbf{M} .
4. We proceed with the analysis as before, with the exception that $P(\mathcal{M}, s|G, \mathbf{g})$ from Equation (A6) is used in place of our previous $P(\mathbf{M}, s|G, \mathbf{g})$. Note the probability $P(s|\mathbf{g})$ of galaxy selection in Equation (40) remains accurate, since selection is made before adding noise to the moments.

More generally we may define a series of b flux bins by bounds f_0, f_1, \dots, f_b , and choose for each bin a distinct covariance matrix \mathbf{C}_A for the added noise (presumably adding zero noise in the lowest-flux bin). For each target galaxy we calculate $P(\mathcal{M}, s|G, \mathbf{g})$ using the value of \mathbf{C}_A we have applied. The non-selection term $P(s|\mathbf{g})$ is calculated using $f_{\min} = f_0$, $f_{\max} = f_b$. The only requirement on the added noise is that it obey the condition $\text{Tr}(\mathbf{B}\mathbf{C}_A) = 0$ which holds for stationary noise.

3. Implementation

We have implemented the BFD shear inference in C++ code. The computational bottleneck of the BFD method is the evaluation of $P(\mathbf{M}, s|G, \mathbf{g})$, which must be done for each target-template

pair. A survey like *DES* might detect $\sim 10^{8.5}$ galaxies, and use $\sim 10^{4.5}$ templates, each replicated over $\sim 10^4$ different translations and rotations, leading to $\sim 10^{17}$ evaluations of $P(\mathbf{M}, s|G, \mathbf{g})$.

Substantial speedup is attained if we can rapidly cull the templates to those which make significant contributions to the sums for P_i , \mathbf{Q}_i , and \mathbf{R}_i , *i.e.* eliminate those highly suppressed by the Gaussian exponential in Equation (38). In this Section we describe some shortcuts to reduce the scale of the problem, and an efficient algorithm for culling the target-template pairs, which leads to an implementation that is feasible to run on modest present-day hardware for even the largest foreseen surveys.

3.1. Computational shortcuts

The target galaxies all have $\mathbf{X} = 0$ by definition of the detection criterion, and so we may first eliminate any template with small $\mathcal{L}(\mathbf{X}^G)$, a criterion we use to bound the displacements \mathbf{u} at which we replicate the templates. Furthermore we have the freedom to rotate the coordinate axes for each target by the angle β which sets one of the ellipticity moments $M_\times = 0$. We must rotate \mathbf{C}_M into this frame, and make sure to rotate all the \mathbf{Q}_i and \mathbf{R}_i back to the original coordinate system after each is calculated. The unlensed population must be invariant under coordinate rotation, so we do *not* have to rotate the \mathbf{M}^G . With this procedure, we can prune the templates to those that are within $\sim 6\sigma$ of $M_\times = 0$. The space $\mathbf{M}^G, \mathbf{X}^G$ of template moments is now bounded to a small interval near the origin in 3 of its 6 dimensions.

3.2. k -d tree algorithm

In building the prior we need to efficiently identify template galaxies with moments \mathbf{M}^G that are close, in moment space, to a given target galaxy \mathbf{M} . The relevant equation is

$$\chi^2 \equiv (\mathbf{M} - \mathbf{M}^G)^T \mathbf{C}_M^{-1} (\mathbf{M} - \mathbf{M}^G) \leq \sigma_{\max}^2. \quad (56)$$

We must be careful in choosing σ_{\max} so that truncation of the integral does not bias \mathbf{g} ; but the number of sampled template galaxies, and the execution time of the measurement, will scale as σ_{\max}^6 .

We choose to store the moments of the template galaxies in a k -d tree (Bentley 1975), which partitions the templates into distinct k -dimensional rectangular nodes that allow for fast lookup of points satisfying (56). The k -d tree is built by assuming a nominal covariance matrix \mathbf{C}_N that is close enough to the \mathbf{C}_M of the targets that the set of templates satisfying (56) with \mathbf{C}_N includes all those which do for \mathbf{C}_M , and not many more. To reduce the number of computations, we do a Cholesky decomposition $\mathbf{C}_N^{-1} = \mathbf{A}^T \mathbf{A}$, and rescale the template and target moments to $\mathbf{N} \equiv \mathbf{A}\mathbf{M}, \mathbf{N}^G \equiv \mathbf{A}\mathbf{M}^G$. This transformation yields $\chi^2 = |\mathbf{N} - \mathbf{N}^G|^2$, the Euclidean distance in \mathbf{N} . The \mathbf{N} are used only to isolate the relevant templates, not to calculate the probabilities.

We need to replicate each template at a grid in \mathbf{u} and rotation angle. The step sizes in translation and rotation are chosen such that \mathbf{N}^G shifts by $\approx \sigma_{\text{step}} \lesssim 1$ between each grid point. Parity-reversed copies are also made. The probability p_G of each template is shared equally between its copies. We discard template copies that have no chance of satisfying Equation (56) for any selected target galaxy (remembering that all selected targets have $\mathbf{X} = 0$, $M_{\times} = 0$, and $f_{\text{min}} < M_f < f_{\text{max}}$).

The derivatives of \mathbf{M}^G with respect to shear are calculated for all retained templates. If all the target galaxies have the same covariance matrix, a number of numerical factors can be precomputed so that they do not need to be recalculated for every template/target pair. Note that a new template set needs to be constructed, and the k -d tree partition repeated, if the target \mathbf{C}_M changes by more than $\approx 10\%$. The construction of the template tree scales as $N_G \log N_G$, where G is the number of templates, which is subdominant to the time $N_t N_G$ for integrating the N_t targets over the template set.

After the tree has been constructed, we find for each target galaxy all the nodes that contain template galaxies with $\chi^2 < \sigma_{\text{max}}^2$ using the nominal \mathbf{C}_N . If the number of templates in the retained nodes exceeds $3N_{\text{sample}}$, we randomly subsample a fixed number N_{sample} of them according to their probabilities p_G . This keeps us from wasting time calculating huge numbers of template/target pairs for targets with large uncertainties, while making full use of the templates that resemble the rarer targets. With this list of template/target pairs, we can calculate the P, \mathbf{Q} , and \mathbf{R} values needed. The speed of the integration step now scales as $N_t N_{\text{sample}}$ if the number of templates becomes large.

Our implementation executes the integration over templates for ≈ 10 galaxies per second per core on a general-purpose cluster, for the GALSIM simulations below in which each target is compared to $\approx 40,000$ templates. At this speed, a 1000-core cluster could measure 10^9 target galaxies (*e.g.* the LSST survey) in just 1 day, probably much faster than the subsequent cosmological inferences will require.

While the BFD method has no parameters to tune to reduce bias, the sampling/integration algorithm has three free parameters— σ_{max} , σ_{step} , and N_{sample} —which trade computational speed and memory requirements against the bias induced by finite sampling. The number N_G of templates sampled from the sky also will be important in controlling finite-sample biases.

3.3. Weights and PSFs

The weight function $W(|k^2|)$ used in calculating the moments of Equation (8) must satisfy two requirements: first, it must vanish at any \mathbf{k} where $\tilde{T}(\mathbf{k}) = 0$, in order to keep measurement errors finite; and it must have two continuous derivatives in order for the shear derivatives of the template moments to be calculable (see Appendix C). With these conditions satisfied, BFD is well-defined and unbiased, but further refinement of W can optimize the noise on the inferred \mathbf{g} and the required

size of “postage stamp” of pixels for the DFT around each galaxy. In our validation tests we use this “ $k\sigma$ ” weight function:

$$W(|k^2|) \equiv \begin{cases} \left(1 - \frac{k^2\sigma^2}{2N}\right)^N & k < \frac{\sqrt{2N}}{\sigma} \\ 0 & k \geq \frac{\sqrt{2N}}{\sigma} \end{cases} \quad (57)$$

with $N = 4$. This closely approximates a Gaussian with width (in k space) of $1/\sigma$, but goes smoothly to zero at finite k .

In our validation tests we assume we have a noiseless, Nyquist-sampled postage stamp of the PSF from which we can measure $\tilde{T}(\mathbf{k})$ on a discrete grid of \mathbf{k} . If we require \tilde{T} at other values of \mathbf{k} , we interpolate the prescription for zero-padding in real space and quintic polynomial interpolation in k -space given by Bernstein & Gruen (2014). This need arises if there is distortion across the image such that either targets or templates are sampled at slightly different pitch than the PSF.

4. Validation

To verify that our implementation of BFD can infer shear with an accuracy of $|m| \lesssim 10^{-3}$, we use two types of simulated data. The “Gauss tests” use Gaussian galaxies, a δ -function PSF, and a Gaussian $W(|k^2|)$, in which case we can calculate all moments and their shear derivatives analytically—no rendering of images is done, so this is fast and bypasses any issues related to image discreteness. The second validation test uses simulated galaxy images produced with the Python/C++ software GALSIM (Rowe et al. 2015).⁵

Table 1 gives the parameters of the two validation simulations. While they use different methods to generate “observed” moments for the target and template galaxies, they use the same integration code. Both simulations proceed as follows:

1. A common galaxy generator is used to generate target and template samples, with shear and noise being applied only to the targets. The galaxies are sampled from a uniform distribution in S/N (Gauss test) or flux (GALSIM test) between specified limits. The galaxy half-light radius r_{50} is also drawn uniformly between two bounds. The (unlensed) ellipticity $e = (a^2 - b^2)/(a^2 + b^2)$ of the source is drawn from the distribution

$$P(e) \propto e(1 - e^2)^2 \exp(-e^2/2\sigma_e^2) \quad (58)$$

and the galaxy position angle is distributed uniformly. Galaxy origins are randomized with respect to the pixel boundaries (if any).

⁵<https://github.com/GalSim-developers/GalSim>

2. A “batch” of measurements is made by generating N_{batch} target galaxies with a constant shear \mathbf{g} , adding noise, and measuring moments about the origin which yields $\mathbf{X} = 0$. Those passing any selection cuts are integrated against N_{template} template galaxies drawn from the same generator, each of which is translated, rotated, and reflected as described above. The P_{tot} , \mathbf{Q}_{tot} , and \mathbf{R}_{tot} for the batch are saved.
3. Batches are processed until we have generated the desired number N_t of target galaxies. Note that each batch draws an independent set of templates. The final shear estimate and its uncertainty are derived from the summed $P, \mathbf{Q}, \mathbf{R}$ using Equations (19) and (18).

4.1. Gauss tests

We use the analytic moments of the Gauss tests to check the BFD formulae and their implementation, and explore the sampling parameters of the integration algorithm. Table 1 describes the baseline simulation; in Section 5 we investigate dependence of shear bias on these parameters using the Gauss tests. Although the moment calculations are analytic, we use the full k -d tree implementation described in Section 3.2 to evaluate the integrals. We can quickly run a sufficient number of statistics to reach the accuracy of $m \sim 10^{-3}$ using these analytic simulations.

Galaxy moments \mathbf{M}^G (and their shear derivatives) are calculated analytically, and the moment noise \mathbf{M}^n is generated from the multivariate Gaussian distribution with the known \mathbf{C}_M . A complication is that the moment noise is held fixed as we shift the target coordinate origin to null the \mathbf{X} moments. This is contrary to the behavior of normal images, and results in some changes to the formulae for $P(\mathbf{D}|\mathbf{g})$ which are described in Appendix B. The baseline Gauss test with 10^9 targets yields $m = (+0.1 \pm 0.4) \times 10^{-3}$.

4.2. GALSIM tests

The GALSIM tests validate several aspects of the code that are not exercised in the Gauss tests, primarily the measurement of moments and PSFs from pixelized images. The GALSIM code is used to produce FITS images, each consisting of 100×100 postage stamps that are 48×48 pixels in size. Every stamp contains one galaxy located near its center. Each galaxy is the sum of an exponential disk and a deVaucouleurs bulge. Both components are given the same ellipticity and half-light radius. The fraction of flux in the bulge component is uniformly distributed between 0 and 1. The center of the bulge is randomly shifted with respect to the center of the disk by a distance up to the half-light radius. For target galaxies, we apply a lensing shear \mathbf{g} . We convolve the final galaxy with an elliptical Moffat PSF. If the galaxies are being used as targets, Gaussian noise is applied to the final stamp image. A selection of targets and templates is shown in Figure 1.

The range of flux assigned to galaxies is set such that it yields $5 < S/N < 25$ for a circular

Table 1. Parameters and results of the baseline validation tests

Characteristic	Gauss test	GALSIM test
Galaxy profile	Gaussian	Decentered disk+bulge
PSF profile	δ -function	Moffat, $\beta = 3.5$
PSF size (pixels)	\dots	$r_{50} = 1.5$
PSF ellipticity	\dots	(0.00, 0.05)
Weight function	Gaussian	$k\sigma$, eqn. (57)
Weight size	$\sigma = 1$	$\sigma = 3.5$ pix
Galaxy radius ¹	0.5–1.5	1.0–2.0
Galaxy S/N	5–25	5–25
σ_e , galaxy shape noise	0.2	0.2
Selection cuts	none	$8 < S/N < 20$
$N_{\text{batch}} / N_{\text{template}}$, target/templates per batch	$10^6 / 3 \times 10^4$	$5 \times 10^5 / 2.5 \times 10^4$
$\sigma_{\text{max}} / \sigma_{\text{step}}$, template truncation/replication	5.5 / 1.0	6.0 / 1.1
N_{sample} , templates subsampled	7×10^4	5×10^4
N_t , total targets	10^9	10^9
Selection fraction	1.0	0.69
\mathbf{g}_{true} , input shear	(0.01, 0.00)	(0.02, 0.00)
$(\mathbf{g}_{\text{meas}} - \mathbf{g}_{\text{true}}) \times 10^5$	$(+0.1, +0.0) \pm (0.4, 0.4)$	$(+4.3, -1.3) \pm (0.9, 0.9)$
Non-linearity α	2	0.5

¹Galaxy half-light radius is given relative to the weight scale for Gauss tests, or relative to the PSF half-light radius for GALSIM tests.

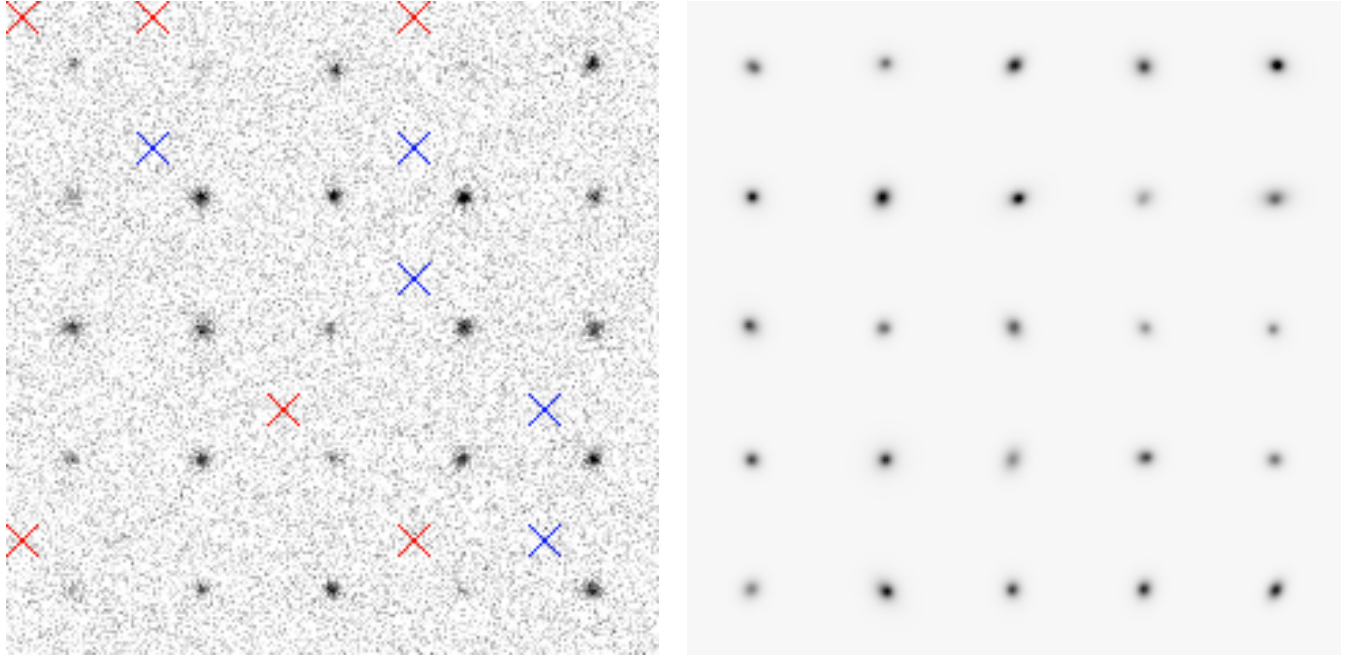


Fig. 1.— A sample of the target (left) and template (right) simulated galaxies used in the validation test. Targets are marked here with an X in the upper left of their stamp if they were cut for low (red) or high (blue) S/N .

galaxy of typical size under matched-aperture detection. In measuring shear, we set selection bounds $f_{\min} = 8\sigma_f$, $f_{\max} = 20\sigma_f$. Note that the selection uses a different definition of S/N than the generation. At fixed flux, the selection favors more compact and more circular galaxies.

The properties for these simulated galaxies were chosen to capture the non-idealities of real data which might affect the BFD implementation:

- We give the PSF an ellipticity $e_2 = 0.05$, which will test our ability to reject PSF asymmetries.
- The Moffat PSF is not strictly band-limited so the data are slightly aliased. The PSF half-light radius of 1.5 pixels yields a sampling equivalent to *DES* imaging in seeing with FWHM of $0''.8$, which would be in the worst-sampled quartile of the data.
- The decentering of the disk and bulge components breaks the perfect elliptical symmetry of the galaxies, which might otherwise be canceling some systematic error in the method.
- Elliptical Gaussians are a six-parameter family, and hence a given point in the 6d $(\mathbf{M}^G, \mathbf{X}^G)$ space has only a single possible value for the shear derivatives. The varying bulge fraction and bulge/disk misregistration in the GALSIM simulations admit a range of shear derivatives at each point in moment space.

- These tests include a non-trivial selection function and hence test the validity of the BFD terms for non-selection.

We produce a total of $N_t = 8.6 \times 10^8$ targets, of which a fraction 0.69105 pass the flux selection test. The calculated $P(s)$ from Equation (40) predicts this extremely well: 0.69111 ± 0.00006 . The uncertainty on $P(s)$ arises from sampling noise in the template set.

Most importantly, the inferred values for g_1 and g_2 imply

$$m = (+2.1 \pm 0.4) \times 10^{-3}, \quad (59)$$

$$c = (-1.3 \pm 0.9) \times 10^{-5}. \quad (60)$$

We detect a deviation from $m = 0$ at 5σ significance: well below that demonstrated by any previous practical method. The c value is within 1.5σ of zero, and suppresses the input PSF ellipticity by a factor of > 3000 .

If we omit the selection terms in Equations (45) and (46), we obtain $m = -0.0122 \pm 0.0004$. The selection term is clearly necessary for part-per-thousand shear inference, and the BFD formalism appears to calculate the correction to 20% accuracy or better.

Lastly we can assess the accuracy of the code’s internal estimates of the uncertainty on the shear estimator. The standard deviation of the g components derived from each batch of targets is $(3.56 \pm 0.04) \times 10^{-4}$, consistent with the internal error estimate from Equation (18) of 3.58×10^{-4} .

5. Testing approximations

We collect here all the assumptions and approximations that have been made in deriving the lensing inference formulae:

1. We have implicitly assumed that we know $\tilde{I}(\mathbf{k})$ at all values of \mathbf{k} with non-vanishing $\tilde{T}(\mathbf{k})$, in other words that we have a Nyquist-sampled real-space image.
2. The pixel noise \mathbf{D}^n is stationary and independent of the underlying galaxy G , and the moment noise likelihood is a multivariate Gaussian.
3. The Jacobian determinant $J = |d\mathbf{X}/d\mathbf{x}_0|$ is positive at any location where there is non-negligible probability of selection
4. Galaxies are uncrowded, in that no other galaxies contribute significantly to \mathbf{M} or \mathbf{X} at any location \mathbf{x} where galaxy G might be selected.
5. The lensing is weak, so that a second-order Taylor expansion about $\mathbf{g} = 0$ captures all information about $P(\mathbf{M}|\mathbf{g})$.

6. Our template set G is a complete sample of source galaxies.
7. We have a noiseless, unlensed image of each template.

In this Section we will describe our progress to date in verifying that failures of these assumptions or approximations will not stand in the way of achieving part-per-thousand inference of \mathbf{g} . Also: our GALSIM simulation results, while very good, are still imperfect, with m measured 5σ deviant from zero. So we are interested in whether any of these approximations could be responsible for this deviation.

5.1. Nyquist sampling

We have implicitly assumed Nyquist sampling of the data by defining our moments as integrals over the regions of \mathbf{k} space with non-vanishing $W(|k^2|)$. We will not in this paper examine the consequences of aliasing in the data due to finite sampling. We do note, however, that the method does not require that the data be available at all \mathbf{k} or even that it be free of aliasing. We can *define* our \mathbf{M} elements to be sums over a finite sampling of \mathbf{k} space, and the formalism remains valid as long as we know what the template galaxies' \mathbf{M}^G would be under the same sampling, and also know the first two derivatives of \mathbf{M}^G with respect to lensing distortion \mathbf{g} . This is true even in the case of aliasing, as long as the templates are aliased in the same way as the targets. This, however, is hard to arrange in practice, and it is better to construct un-aliased data from dithered images if necessary, as described in a simple case by Lauer (1999) and in a more general case by Rowe et al. (2011).

Note also that the Moffat PSF used in the validation tests of Section 4 is not strictly band-limited, so these tests incurred a level of aliasing that would be typical for a well-designed ground-based survey. In future tests we will evaluate whether this aliasing, or some other approximation in the GALSIM rendering, is causing the non-zero m value in the GALSIM tests.

5.2. Stationary noise

The assumption of stationary, source-independent noise is valid for background-limited (or read-noise-limited) imaging, which will generally be the case for the galaxies dominating the lensing information in ground-based weak-lensing surveys. We leave for future work the investigation of the impact of shot noise from source photons, which may be relevant for low-background space-based surveys. Our current simulations do not include source shot noise.

5.3. Convex galaxies

The assumption of positive Jacobian determinant J for all selectable regions was necessary to render as feasible the analytic integration of selection probability, and also to avoid calculating the joint probability of multiple detections of the same source. We consider two potential modes of failure of this approximation.

First, if the galaxy is sufficiently faint, J^G is small enough even near its peak that the noise in \mathbf{M} can flip the sign and create a fold in the $\mathbf{x} \rightarrow \mathbf{X}$ mapping. Clearly the defense against this is to have the selection threshold f_{\min} be large enough ($\gtrsim 5\sigma_f$) that J^G is also large enough to dominate the noise fluctuations. Further work is needed to determine if there is a level of f_{\min} which satisfactorily suppresses noise detections without discarding sources that carry a significant fraction of the lensing information.

Second, there will be galaxies which have high flux but have complex structure such that J^G crosses or approaches zero because of multiple maxima or plateaus. We should note that we only care about the structure in the galaxy *after* it has been smoothed by the detection filter, which in real space is the Fourier transform of $W(|k^2|)/\tilde{T}(\mathbf{k})$. We will usually aim to have $W \approx \tilde{T}^2 \tilde{I}^g$, where $\tilde{I}^g(\mathbf{k})$ is the transform of the average observed galaxy. Thus in practice, the observed image, already convolved by the PSF, is convolved again with the PSF and the typical galaxy profile before running the detection scheme. This means that any maxima or plateaus on scales of the PSF or smaller are going to be erased.

We have not yet validated BFD on sources with well-resolved structure that might lead to multiple selections, but our implementation includes some ameliorative measures in anticipation of the issue. First, in our postage-stamp tests, we can discard all but the highest-flux detection in each stamp. Our calculation of $P(\mathbf{M}, s|G, \mathbf{g})$ should then incorporate the probability of a higher-flux selection existing. Our crude version of this is to include in our sum over \mathbf{u} only those values of \mathbf{u} that have $J^G \geq 0$ and are contiguous with global maximum for f . In other words we assume that the brightest detection will arise from the convex region of the (filtered) galaxy that surrounds the global maximum. We have not yet quantified the efficacy of this approach on realistic galaxies.

5.4. Uncrowded galaxies

Overlapping galaxies pose a considerable challenge for BFD (and indeed for nearly all lensing-measurement methods). We have strived for a formalism that makes minimal assumptions about the morphology of the galaxies. But galaxy image deblending depends fundamentally on having some prior expectations for galaxy morphology in order to partition the flux in a single pixel among two (or more) sources. We suspect that for mild cases of blending, one could precede the BFD analysis with joint model-fitting to multiple overlapping sources; and then, subtract each source model in turn when measuring the Fourier moments of the other. This would likely be successful

as long as the subtracted flux has moments that are small compared to the remainder, as our dependence on the correctness of the model will remain weak. At present, we will simply ignore galaxies which overlap to an extent that they grossly perturb each other’s moments. Crowding remains as a critical issue for deep ground-based surveys, where the product of typical observed galaxy size and desired target number density is $\gtrsim 0.1$ (Chang et al. 2013).

5.5. Weak lensing limit

Any shear estimator that is analytic in the input shear and introduces no preferred direction on the sky should have

$$\langle \mathbf{g}_{\text{meas}} - \mathbf{g}_{\text{true}} \rangle = [m + \alpha g^2 + O(g^4)] \mathbf{g}_{\text{true}}. \quad (61)$$

The coefficient α is expected to be of order unity unless $d \log P / d\mathbf{g}$ becomes large for some targets. This will occur only for galaxies whose moments are many σ different from any of the templates, a situation we avoid by adding noise to high- S/N targets. If $\alpha \sim 1$, then the desired accuracy of $< 10^{-3}$ of the shear will be lost in the second order Taylor expansion about $\mathbf{g} = 0$ for $g \gtrsim 0.03$. Expanding around $g \neq 0$ greatly complicates the calculation of the moments and their derivatives, making it impractical. BA14 derive third-order expressions, but these are not included in our present implementation and would also slow the method substantially.

Figure 2 shows the recovered multiplicative bias as a function of input shear in tests for non-linear behavior of both the Gauss and GALSIM tests. The bias is consistent with the expected quadratic growth with g , with $\alpha \approx 2$ and ≈ 0.5 in the two case. A similar result is obtained for a model-fitting implementation of the BA14 by Sheldon (2014). The value of α clearly can vary based on the nature of the galaxies and the noise levels. The $\alpha = 0.5$ nonlinearity contributes an apparent multiplicative error of $\alpha g^2 = 0.2 \times 10^{-3}$ to our principal GALSIM test results, smaller than the measurement error even with 10^9 target galaxies. But if real cosmic-shear measurements have a value closer to the $\alpha = 2$ seen in the Gauss tests, the nonlinearity cannot be ignored: The cosmic-shear test is, at its most basic, a measure of the RMS dispersion σ_g of the point distribution function (PDF) of shear to $z \sim 1$ sources. Propagating (61) through a nearly-Gaussian PDF suggests that we would mis-estimate σ_g by a factor $1 + 3\alpha\sigma_g^2$, which for $\sigma_g \approx 0.02$ and $\alpha = 2$ would be a fractional error of 0.0024 on σ_g , larger than the expected statistical error for future surveys, and in need of a correction. Fortunately the value of α is straightforwardly assessed to the $\sim 20\%$ accuracy that would be needed to render nonlinearity errors negligible.

The nonlinearity poses a potentially larger problem for regions of high shear such as galaxy clusters. This problem can be overcome with an iterative procedure if we are fitting a model to the shear. We first fit the model, ignoring nonlinear shear response. In regions of not-so-weak shear, *e.g.* where the shear is ≈ 0.1 , we can unshear the source galaxy by the predicted 0.1 shear before measuring its moments and calculating P_i , \mathbf{Q}_i , and \mathbf{R}_i with the nominal second order procedure. This will yield a Taylor expansion of $P(\mathbf{D}_i|\mathbf{g})$ of deviations from the model, which can then be

used to refine the model. We speculate that this procedure would recover full unbiased accuracy around well-measured individual clusters.

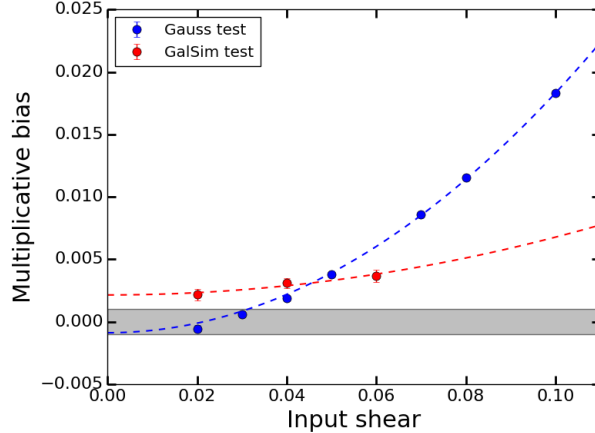


Fig. 2.— The recovered multiplicative bias using the second-order BFD formalism, as a function of input shear. The grey band shows the desired accuracy of $m < 10^{-3}$. The dashed line is a fit of the data to the expected quadratic dependence on g , with coefficient $\alpha \approx 2$ for the Gauss tests and $\alpha \approx 0.5$ for the GALSIM tests.

5.6. Noiseless, unlensed templates

We have assumed that the galaxies used in constructing the prior are noiseless and unlensed, whereas in real data they will be both noisy and lensed by large scale structure. We run a series of Gaussian simulations to evaluate the impact of each of these on shear measurement. In the first test, we add noise to the moments and derivatives of the template galaxies. Figure 3 shows the bias in recovered shear as a function of the ratio of template noise variance to target noise variance. When this ratio is $\sim 10\%$, the multiplicative bias remains $< 10^{-3}$. Therefore, observations with $> 10\times$ the integration time of target galaxies are sufficiently high- S/N to use as “noiseless” template galaxies. Most current and future lensing surveys already include such deep observations to maximize their scientific value.

In the second test, we assess the impact of using template galaxies that have already been sheared. Recall that we use rotated copies of all observed templates, which means that the *mean* shear on our templates is always zero, but we must ask whether non-vanishing *variance* of the shear on the templates produces biased shear inferences. We applied shear to the templates in two different ways: a constant shear amplitude for every template; and a shear randomly drawn from a zero mean Gaussian with dispersion σ_g . Fig 3 shows the bias as a function of the applied template shear. The multiplicative bias satisfies $|m| < 10^{-3}$ in both cases if the RMS template shear is < 0.04 . The typical shear imparted by large scale structure is only half as large, thus it appears

feasible to use deep integrations of the real sky to produce the template set.

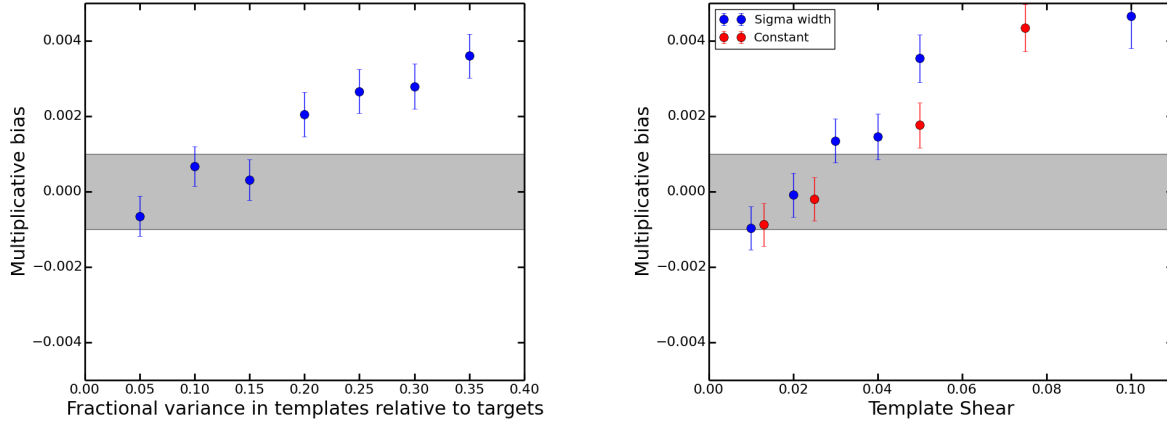


Fig. 3.— At left: the multiplicative bias in shear inferred from simulations where we add noise to the template galaxies. The x axis gives the noise variance on the templates relative to the noise variance on the target observations. At right: the multiplicative bias recovered when template galaxies have an applied shear that is either constant or drawn from a Gaussian of given RMS value. The grey band shows the desired accuracy of $m < 10^{-3}$, which we see is retained when the templates have $\lesssim 10\%$ of the noise power of the targets, and the RMS shear on templates is $\lesssim 0.04$.

5.7. Complete template set

We approximate the integral over all possible template galaxy types and locations with a finite number N_{template} of high- S/N galaxies, and by using a finite number of copies of each at intervals of σ_{step} in translation and rotation. Further we subsample a number N_{sample} of the resultant copies that lie within σ_{max} , of each target. Ideally, the variance due to these approximations will be far below the expected noise of the targets. BA14 suggest that BFD estimates will have a bias that scales inversely with the number of templates. We again use the Gauss tests to see how sensitive the recovered shear is to N_{template} and N_{sample} . Figure 4 shows that, for the Gauss tests, the bias is within $|m| < 10^{-3}$ when we have at least 30,000 template galaxies and $N_{\text{sample}} \gtrsim 70,000$. The necessary values will in practice depend on how the galaxies are distributed in moment space, how noisy they are, and how we implement the added-noise strategy of Section 2.5. These tests suggest, though, that a sample of 10^4 – 10^5 deep sky templates will suffice. This is readily attainable in all planned surveys.

The GALSIM tests reported in Section 4 used a value of $N_{\text{template}} = 2.5 \times 10^4$. Tests with a $2.5 \times$ smaller value show no significant change in m , arguing against the hypothesis that our non-zero m value is attributable to insufficient template sampling. Figure 5 shows that for the GALSIM tests, we integrate over a similar number of templates ($\approx 40,000$) for each target. Note that in this case

N_{samp} was 50,000, so we never invoked the subsampling of accessible templates. An unrealistic aspect of this test is that galaxies are uniformly distributed in flux, leading to uniformity in the number of templates. The real sky has fewer bright galaxies and we would expect the template count to increase for fainter sources.

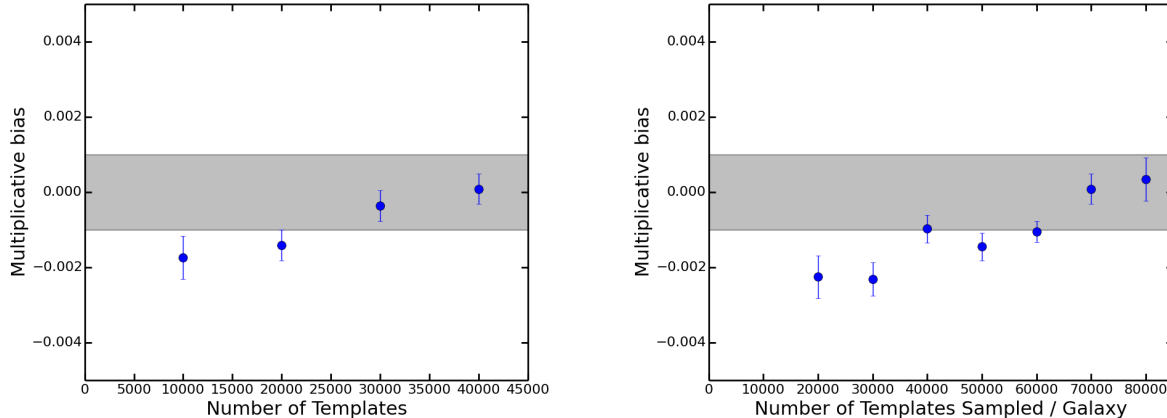


Fig. 4.— The multiplicative bias recovered as a function of the number of initial template galaxies before adding rotated/translated copies (left) and as a function of N_{sample} (right), the number of subsampled templates used to evaluate the integrals for each target galaxy. The grey band shows the desired accuracy of $|m| < 10^{-3}$.

6. Future developments

The BFD formalism can be straightforwardly extended beyond the basic single-image, single-plane shear-estimation implementation that we test in this paper. In this section we sketch some of these possibilities.

6.1. Interferometric data

Interferometric data is collected in Fourier domain; data for a galaxy will consist of estimates of $\tilde{I}(\mathbf{k})$ (the visibilities) at a finite sampling of \mathbf{k} values determined by the interferometer baselines. As noted in Section 5.1, it is not required that we measure galaxies at all \mathbf{k} : we can replace the integrals over d^2k in Equation (8) with weighted sums over the visibilities. The sole requirement is that we be able to calculate the same sums for the template galaxies, as well as derivatives under lensing distortion.

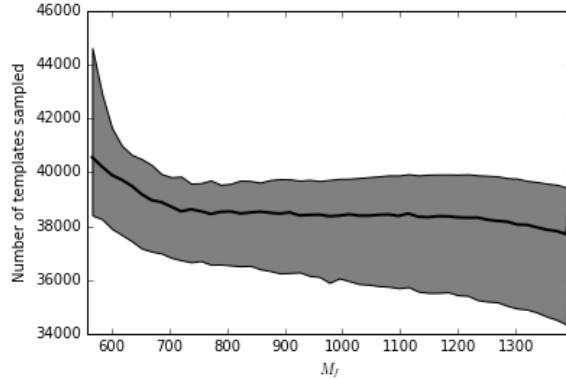


Fig. 5.— The number of templates used in the integration of $P(\mathbf{D}_i|\mathbf{g})$ for each galaxy as a function of its flux moment M_f in the GALSIM tests. The central line is the median, the shaded region bounds the 10–90 percentile range.

6.2. Multi-image analysis and multi-band data

Equation (8) defines our compressed measurement vector \mathbf{M} as derived from a single image $I(\mathbf{x})$ observed with a single PSF $T(\mathbf{x})$. In most surveys, observations of a given target will be spread over multiple exposures $i \in \{1, 2, \dots, N\}$. As long as each individual exposure is unaliased, we can define the moments of the target as a weighted sum over the moments \mathbf{M}_i measured on each exposure:

$$\mathbf{M} = \sum_i w_i \mathbf{M}_i. \quad (62)$$

(and likewise for the detection moments \mathbf{X}). It is important that the w_i be determined independent of the observed properties of the galaxy, so that the probability $P(\mathbf{M}|G)$ remains calculable. This linear combination of the \mathbf{M}_i yields a zero-mean normal distribution for the moment noise, with covariance matrix \mathbf{C}_M that is the sum of those for the individual exposures weighted by w_i^2 . Our implementation of this extension selects the weights to minimize the variance of the ellipticity moment M_+ , a process which depends only on the noise level and PSF of each exposure.

Formally, we can choose a different weighting function $W(|k^2|)$ for each exposure, as long as we can calculate the \mathbf{M}^G that would result for each template (and its lensing derivatives). It is, however, convenient to use the same W for all exposures, simplifying construction of the template set. If the seeing conditions of the exposures vary widely, then a single W may be far from optimum for some exposures; but since poor-seeing exposures carry less lensing information to begin with, we lose little by selecting W to optimize the use of exposures at median or better seeing.

Because we make use of un-normalized moments, it is important that all exposures (including templates) be placed on a common photometric scale.

6.2.1. Multiple observing bands

There is also no requirement that all exposures be taken through the same filter. Equation (62) can refer to exposures in multiple filters. We must once again select weights in advance—iterative procedures such as weighting each galaxy according to its observed colors result in $P(\mathbf{M}|G)$ functions that are analytically intractable. Choosing fixed weights to apply to each filter is akin to measuring moments in a bandpass that is the weighted sum of all the filters’ bandpasses.

Another alternative would be to define the moment vector \mathbf{M} to be the concatenation of moment vectors from each filter. This retains more information, though at the cost of higher memory and computation demands due to the higher-dimensional moment space. We advocate a hybrid procedure, in which we retain distinct flux moments $M_{f,i}$ for each filter i , but retain only a single weighted combination of the other moments $M_r, M_+, M_\times, \mathbf{X}$. This is because shape information is generally highly degenerate between bands (Jarvis & Jain 2008), but colors carry a lot of information. For example, red galaxies have a more compact shape distribution than blue at low redshift (Bernstein & Jarvis 2002), so retaining color information when we compress the pixel data allows the BFD formalism to exploit this distinction for more precise shear inference.

Again the key requirement is that a low-noise measure of the template moments \mathbf{M}^G be available, as is the case if the templates are observed in all of the same bands as the targets. One can select distinct W functions for each band, as long as the targets and templates are treated consistently. An advantage of a fixed W across bands is that the resultant flux moments then have the same pre-seeing window function on the galaxy in all bands. This property, also attainable with PSF-matching codes, or the GAAP algorithm of Kuijken (2008), is desirable for use with photometric redshifts, since it insures that the measured colors correspond to a fixed weighting of the stellar populations in the galaxy, *i.e.* we are not mixing aperture effects with stellar evolution.

6.3. Star-galaxy discrimination

Stars are Dirac δ functions in real space, so their moments \mathbf{M}^G are known functions of flux and position \mathbf{x}_G . Furthermore they are unaffected by cosmological-scale lensing so we set the lensing derivatives of \mathbf{M}^G to zero. If we add stellar sources to our template set, assigning them p_G values according to a prior expected sky density vs flux, then we automatically correct the shear estimate for dilution by stellar sources. We obtain as a by-product an excellent posterior estimate of the probability that each source is stellar, and we can sum these to obtain a posterior stellar density estimate which may help to refine the stellar model that led to the prior.

It should also be noted that faint galaxy targets which might be confused with stars are by definition weakly resolved, and contribute very little to \mathbf{Q}_{tot} and \mathbf{R}_{tot} for shear estimation. Hence the shear estimation will have low sensitivity to mis-estimation of the stellar density in the prior.

If we have observed in multiple filters and retained flux moments $M_{f,i}$ in each band as described

in Section 6.2.1, we can (and must) produce stellar templates across the color-magnitude diagram, with p_G values expressing the expected density vs color and magnitude.

6.4. Magnification

The BFD formalism makes no assumptions about the nature of the lensing distortion vector \mathbf{g} , except that we can simulate its action on each template, and that $P(\mathbf{D}|\mathbf{g})$ is well approximated by a quadratic Taylor expansion. This means that we can include magnification μ along with the shear components g_1 and g_2 with essentially no change except to increment the dimension of the \mathbf{Q} and \mathbf{R} derivatives.

Huff & Graves (2014) note that early-type galaxies define a narrow plane in the space of flux, size, and concentration, which then enables much-enhanced determination of magnification. Our current BFD implementation would not exploit this gain since our compressed data vector lacks information on concentration. This could be remedied by adding a $|k^4|$ moment to \mathbf{M} . Furthermore we would need color information, *i.e.* the series of flux moments proposed in Section 6.2.1, to distinguish red galaxies in a desired redshift range. There is no need to “teach” BFD about the existence of the Huff-Graves relation. Any such relation that exists will be automatically exploited in the lensing constraints, as long as the action of lensing produces a shift in the way the galaxies populate the moment space.

Two minor technical points about the estimation of magnification: first, Equation (53) has assumed that galaxies are placed by a Poisson process. Clustering of sources will mean that the resultant posterior is invalid, underestimating the uncertainty on μ . We can, if desired, treat the unlensed density n as a spatial variable when inferring magnification statistics, to distinguish clustering from magnification. Second, recall that magnification will dilute the source population on the sky, changing the apparent n . This effect is already included in our implementation because we calculate the derivative $\partial \mathbf{M}^G / \partial \mu$ by magnifying about the coordinate origin, not the center of the galaxy. This means that our grid \mathbf{u} of template copies is dilated by magnification, but we do not alter $\Delta^2 u$ in Equation (38) or Equation (40). Thus source dilation is included in the P terms, and the n term should retain the unlensed density.

Higher-order lensing distortions, *i.e.* flexions, can similarly be constrained by the BFD method, again as long as we augment the compressed data vector to include quantities that are altered at first order by the distortion. Since flexion is not an affine transformation, its action on the Fourier domain $\tilde{I}(\mathbf{k})$ is less easily expressed than shear and magnification. Nonetheless, it is possible to derive flexion derivatives of template moments for simultaneous constraint of all these lensing distortions using BFD.

6.5. Lensing tomography and photometric redshifts

One important caveat to BFD is that one cannot select subsets of the targets and then combine their $P_i, \mathbf{Q}_i, \mathbf{R}_i$ values to estimate the shear on this subset. This would invalidate the $P(\mathbf{D}|\mathbf{g})$ formulae we have derived, unless one can guarantee that the *post hoc* selection criteria do not at all alter the distribution of underlying moments \mathbf{M}^G of the selected galaxies.

Many useful scientific inferences and diagnostic tests for weak lensing measurements rely upon comparing \mathbf{g} on subpopulations of the sources. Most critically, the bulk of the lensing information, plus constraints on contamination by intrinsic galaxy alignments, require splitting the source population into redshift bins, a.k.a. lensing tomography.

If precise redshift estimates are available for all targets and templates, then the application of BFD is straightforward, as we compare each target only to templates that reside in the same redshift bin. More commonly we have *probabilistic* redshift estimates for targets derived from photometric redshift (photo- z) estimation. Partitioning target or template galaxies by their maximum-likelihood redshifts will not, in general, yield valid BFD inferences on the shear in each redshift bin.⁶

This apparent stumbling block turns out to be an opportunity: the BFD formalism contains within it an ideal Bayesian photo- z estimation mechanism, particularly for the sources with modest $S/N \lesssim 30$ photometry that dominate the weak lensing information in most surveys. Benítez (2000) presents the formalism for Bayesian inference of redshift from broad-band fluxes; like BFD, it relies upon having noiseless data vectors for a sample of “truth” objects of known prevalence on the night sky.

We generalize the BFD method as follows: the lensing vector is extended to the tomographic information $\mathbf{t} = \{\mathbf{g}_1, \dots, \mathbf{g}_Z\}$, where \mathbf{g}_ν is the lensing distortion applied to sources in redshift bin ν out of Z total bins. We want the posterior $P(\mathbf{t}|\mathbf{D})$, and as before we compress the image data \mathbf{D} into the moments \mathbf{M}_i of objects detected and selected at positions \mathbf{x}_i . The posterior on \mathbf{t} is calculable once we have expressions for $P(\mathbf{M}_i, s|\mathbf{t})$ and the total selection probability $P(s|\mathbf{t})$. If we know the probability $p_{G\nu}$ that template galaxy G is in redshift bin ν , then we have the clear generalization of Equation (38) to the tomographic case:

$$P(\mathbf{M}, s|\mathbf{t}) = \sum_{G, \mathbf{x}_G} p_G \Delta^2 u \sum_{\nu} p_{G\nu} P(\mathbf{M}, s|G, \mathbf{u}, \mathbf{g}_\nu) \quad (63)$$

$$P(\mathbf{M}, s|G, \mathbf{u}, \mathbf{g}_\nu) = |J(\mathbf{M})| \mathcal{L}[\mathbf{X}^G(\mathbf{u}, \mathbf{g}_\nu)] \mathcal{L}[\mathbf{M} - \mathbf{M}^G(\mathbf{u}, \mathbf{g}_\nu)] \quad (64)$$

In the second line we make explicit the dependence of the template moments on its true position \mathbf{u} relative to the detection location and upon the shear \mathbf{g}_ν to the source. The total probability of detection vs \mathbf{t} is similarly obtained by introducing $p_{G\nu}$ into Equation (40).

⁶The same is true for most other lensing-inference methods: the responsivities or empirical calibrations they employ will depend upon the galaxy selection in subtle ways that may thwart part-per-thousand calibration.

We can also easily calculate the posterior redshift distribution $P(\nu|\mathbf{M}_i)$ for each source, which would be found equivalent to the treatment of Benítez (2000). Of course our redshift discrimination will be weak unless we have measured flux moments $M_{f,j}$ in multiple bands j as described in Section 6.2.1, where we noted that our pre-seeing aperture-matched fluxes are ideal for photo- z purposes. We also note that we are working with fluxes, not colors, and therefore we automatically include the “luminosity prior” that is often added by hand into photo- z estimators. Indeed our inclusion of M_r , M_+ , and M_\times means that we automatically exploit any size, surface brightness, or ellipticity information that helps with redshift discrimination.

Extending BFD to return the full tomographic lensing likelihood $P(\mathbf{t}|\mathbf{D})$ would have many advantages for precision lensing cosmology. It would allow us to extract all the available lensing information from galaxies with low-resolution photo- z information due either to color ambiguities or low S/N . It eliminates the need for *post hoc* estimation of selection biases induced on the lensing estimators by photo- z cuts. An important issue will be whether it is feasible to use sufficiently many, narrow bins that we do not need to worry about the variation of lensing signal across the redshift range of a bin.

The implementation of BFD tomography requires that we have a template galaxy set with known redshift probabilities assigned to each. Clearly one issue is how to obtain this information—especially since the number of templates required to sample the moment space with desired density will increase substantially with additional flux dimensions in \mathbf{M} . It is likely infeasible to obtain spectroscopic redshifts for a sufficiently large and complete set of templates. A survey such as *DES* which observes galaxies in the *grizY* bands requires higher- S/N observations in these bands to create the template moments set; these observations in the survey bands could be supplemented with deep data in other bands and with other instruments to tighten the $p_{G\nu}$ estimates for the template set—for example, the COSMOS field has data in many bands across the EM spectrum, producing much higher-reliability photo- z ’s beyond the spectroscopic limit (Ilbert et al. 2009). It will likely be necessary to use spectral-synthesis methods to create artificially redshifted copies of the observed template galaxies, just as we synthesize \mathbf{M}^G for rotated copies, in order to more densely sample the template space and damp the line-of-sight structures (sample variance) present in the template fields. We envision BFD primarily as a means to rigorously bootstrap the photo- z calibration from a well-observed subset of galaxies to the full survey population.

Incompleteness in the spectroscopic surveys defining the redshift priors is a difficult problem (see *e.g.* Bernstein & Huterer 2010). The BFD tomography formalism allows us to propagate the uncertainties due to missed redshifts into the final cosmological results: we can reassign the probabilities $p_{G\nu}$ using different assumptions about the missing redshifts, and propagate these cases through $P(\mathbf{t}, \mathbf{D})$ into cosmological inferences to determine their impact. One could also add a “mystery bin” to \mathbf{t} to which we assign all template galaxies with poorly known redshift. The tomographic BFD formalism will calculate the likelihood that any given target has unknown z , and cosmological inferences could marginalize over the redshift distribution of the mystery bin.

Joint BFD tomography and photo- z is clearly an intriguing and critical extension of the method, with quite a few details to work out. We will examine these in future publications.

7. Conclusion

The BFD method is now a practical, validated means to estimate WL shear at parts-per-thousand accuracy. In our initial large-scale tests, deviations from perfection were measurable only with trials of nearly 10^9 simulated galaxies. Work remains to determine if and why BFD has inaccuracies at the level of $m = 0.002$. Future work will investigate the possible impact of aliasing, and approximations in the rendering of images onto finite postage stamps, since we find m consistent with zero for our Gauss tests that do no rendering. PSF asymmetries are perfectly removed from the shear estimator, to present accuracy. We have implemented a flux selection in such a way that we can correct the $> 1\%$ selection bias induced on the shear. The BFD formalism needs no parameter tuning or calibration to eliminate biases—there is just a free weighting function one chooses to minimize noise. A real implementation does have some parameters for sampling the infinite distribution of galaxies on the sky, which imply a tradeoff of bias vs observational and computational resources. We have used simulations to validate the performance of the method and demonstrate that the desired accuracy is attainable with readily available resources to sample the underlying galaxy population.

While BFD assumes that noiseless images of unlensed galaxy populations are available, our tests indicate that it retains desired accuracy when the templates are taken from images with the same instrument, but $\approx 10\times$ longer exposure time than the target survey. This is eminently practical, and indeed most planned surveys already have such “deep fields” for other reasons.

The BFD method also predicts the uncertainty on the shear estimate, and the detection efficiency, correctly to within the shot noise of our tests. The algorithms should scale to the needs of even the largest proposed surveys, and the computational steps are simple, highly parallel and amenable to execution on GPU’s if greater speed is needed.

Sheldon (2014) reports $|m| < 2 \times 10^{-3}$ when applying the BA14 formalism to likelihoods derived from MCMC model-fitting to galaxy images with S/N as low as 10. The galaxy images were both drawn and fitted with simple Sérsic models, so this work notes that the method may be susceptible to “model bias” in more realistic cases. Sheldon (2014) also does not yet include a prescription for galaxy selection and resultant biases.

The only other demonstration of part-per-thousand WL inference at $S/N \lesssim 10$ from a realistic algorithm of which we are aware is Zhang et al. (2015), also implemented as the FOURIERQUAD method in the GREAT3 challenge (Mandelbaum et al. 2015). This method shares several characteristics with BFD: galaxies are reduced to weighted moments in Fourier space, where PSF correction is straightforward. Neither method assigns shapes to individual galaxies; FOURIERQUAD works by stacking un-normalized moments of the power spectrum; the shear estimator is a quotient of

stacks. Using the power spectrum has the advantage of making the estimator insensitive to choice of galaxy origin, but amplifies measurement noise by $\sqrt{2}$ relative to our phase-sensitive moments. More problematic is that a stacking method weights galaxies by flux, which is far from optimal. FOURIERQUAD does not yet have an approach to selection and weighting of sources without biasing shear inferences. BFD is at this time closer to applicability on real data.

Schneider et al. (2015) propose an ambitious effort to simultaneously model the shear field, the pixel-level appearance of galaxies within it, and the underlying distribution of the source galaxies. This approach shares some formalism with BFD, but does ultimately rely on parametric models for the galaxies. Our “model,” which is that galaxies’ true moments are equal to those of galaxies found in a deep sub-survey, should be less subject to model bias than the Schneider et al. (2015) approach while greatly reducing the computational complexity.

There are issues to address before BFD can be applied to real survey data. Working in Fourier space means we cannot easily exclude pixel data contaminated by cosmic rays or defects, and hence we need some method for infill of pixels or rejection of exposures. Overlapping or multi-peaked galaxy images are not handled by BFD, so we will need some combination of model-based deblending with rejection of hopeless overlaps that does not significantly bias WL inferences. This will be easier in low-density surveys such as *DES* and *KiDS* than deep ground-based surveys such as *LSST* and *HSC*. For space-based surveys, we need to investigate the behavior of BFD in the presence of source shot noise that violates our background-limited (stationary) noise assumption. We also may need to develop a nonlinearity correction for some applications.

Our validation tests assume constant shear across all galaxies, but as BA14 point out, it is straightforward to calculate a posterior likelihood on the parameters of any model of shear vs position, for example for tangential shear vs radius around a selected lens population. Cosmological models, however, predict a power spectrum or other statistical property of the WL field rather than predicting the shear pattern itself. Current 2-point (and 3-point) estimators for shear assume that each source galaxy provides a point estimate of the shear, but BFD returns a different kind of information, namely some weak probability distribution for shear along each line of sight in the form of $\{P_i, \mathbf{Q}_i, \mathbf{R}_i\}$. Exploitation of the BFD outputs for lensing statistics will require development of new estimation frameworks. Madhavacheril et al. (2015) discuss means to treat such outputs as point estimators, and quadratic estimators for 2-point functions that use BFD-style information.

We have also treated the lensing distortion as a single screen, whereas the sources are distributed in z and hence we measure a weighted mean of shear on the line of sight. A real experiment will need to estimate the z distribution of sources—or more precisely, the distribution of contribution to the BFD shear estimate. Better yet, we have outlined an extension of BFD to joint Bayesian redshift and shear estimation, which directly generates a tomographic lensing likelihood $P(\mathbf{D}_i|\mathbf{t})$ for each source where \mathbf{t} contains the shear (and potentially magnification and source density) at a series of z bins. This could open the door to full exploitation of the low-to-modest S/N regime—where both photo- z and WL estimators have proven difficult to produce without bias—that potentially

carries more information than high- S/N galaxies with well-constrained photo- z 's. Work is needed to develop statistics to constrain cosmological models with this $P(\mathbf{D}_i|\mathbf{t})$ information, as opposed to the binned point estimates used now. It is likely that there are extensions of the Madhavacheril et al. (2015) techniques to this tomographic case.

A critical question will be how many template galaxies must be observed, particularly in the tomographic case where we will need to increase the dimensionality of the moment space that the templates sample. This is related to the question of how large and complete a spectroscopic sample is needed to calibrate photo- z 's to the accuracy needed for WL cosmology.

The BFD method also naturally extends to multi-filter or interferometric observations, and deals gracefully with the blurring of the stellar and galactic loci in faint surveys. Compared to currently dominant model-fitting methods for WL inference, BFD has some disadvantages, such as not-quite-optimal use of the pixel information, annoyances with defective pixels, and a less-clear route to using crowded sources. BFD's advantages are, however, substantial, primarily in the superior accuracy that comes from having a first-principles treatment of noise and selection, and no need to assume a functional form for the sources.

We thank Michael Jarvis, Rachel Mandelbaum, and Barney Rowe for leading the development of the excellent GALSIM package, and thank them plus Erin Sheldon for their advice on the BFD work. Our referee Joe Zuntz improved this paper as well. This work was supported by grants AST-1311924 from the National Science Foundation, DE-SC007901 from the Department of Energy, NNX11AI25G from NASA, and cooperative agreement with JPL under NASA grant ROSES-12-EUCLID12-0004. RA acknowledges financial support from Princeton University.

REFERENCES

- Amara, A., & Réfrégier, A. 2008, MNRAS, 391, 228
- Benítez, N. 2000, ApJ, 536, 571
- Bentley, J. L. 1975, Communications of the ACM, 18, 509
- Bernstein, G. M. 2010, MNRAS, 406, 2793
- Bernstein, G. M., & Armstrong, R. 2014, MNRAS, 438, 1880 [BA14]
- Bernstein, G. M., & Gruen, D. 2014, PASP, 126, 287
- Bernstein, G., & Huterer, D. 2010, MNRAS, 401, 1399
- Bernstein, G. M., & Jarvis, M. 2002, AJ, 123, 583
- Chang, C., Jarvis, M., Jain, B., et al. 2013, MNRAS, 434, 2121

- Chang, T.-C., Refregier, A., & Helfand, D. J. 2004, *ApJ*, 617, 794
- Das, S., Louis, T., Nolta, M. R., et al. 2014, *J. Cosmology Astropart. Phys.*, 4, 014
- Demetroullas, C., & Brown, M. L. 2015, *arXiv:1507.05977*
- Giannantonio, T., Fosalba, P., Cawthon, R., et al. 2015, *arXiv:1507.05551*
- Gruen, D., Seitz, S., Koppenhoefer, J., & Riffeser, A. 2010, *ApJ*, 720, 639
- Huff, E. M., & Graves, G. J. 2014, *ApJ*, 780, L16
- Huterer, D., Takada, M., Bernstein, G., & Jain, B. 2006, *MNRAS*, 366, 101
- Ilbert, O., Capak, P., Salvato, M., et al. 2009, *ApJ*, 690, 1236
- Jarvis, M., & Jain, B. 2008, *J. Cosmology Astropart. Phys.*, 1, 003
- Jarvis, M., Sheldon, E., Zuntz, J. et al. 2015, *arXiv:1507.05603*
- Kacprzak, T., Zuntz, J., Rowe, B., et al. 2012, *MNRAS*, 427, 2711
- Kaiser, N., Squires, G., & Broadhurst, T. 1995, *ApJ*, 449, 460
- Kuijken, K. 2008, *A&A*, 482, 1053
- Kuijken, K., Heymans, C., Hildebrandt, H. et al. 2015, *arXiv:1507.00738*
- Lauer, T. R. 1999, *PASP*, 111, 227
- Laureijs, R., Amiaux, J., Arduini, S., et al. 2011, *arXiv:1110.3193*
- Madhavacheril, M. S., McDonald, P., Sehgal, N., & Slosar, A. 2015, *J. Cosmology Astropart. Phys.*, 1, 022
- Mandelbaum, R., Rowe, B., Armstrong, R., et al. 2015, *MNRAS*, 450, 2963
- Miller, L., Heymans, C., Kitching, T. D., et al. 2013, *MNRAS*, 429, 2858
- Planck Collaboration, Ade, P. A. R., Aghanim, N., et al. 2015, *arXiv:1502.01591*
- Rowe, B., Hirata, C., & Rhodes, J. 2011, *ApJ*, 741, 46
- Rowe, B. T. P., Jarvis, M., Mandelbaum, R., et al. 2015, *Astronomy and Computing*, 10, 121
- Schneider, M. D., Hogg, D. W., Marshall, P. J., et al. 2015, *ApJ*, 807, 87
- Sheldon, E. S. 2014, *MNRAS*, 444, L25
- Takada, M. 2010, *American Institute of Physics Conference Series*, 1279, 120; see also <http://subarutelescope.org/Projects/HSC/surveyplan.html>

van Engelen, A., Keisler, R., Zahn, O., et al. 2012, *ApJ*, 756, 142

Voigt, L. M., & Bridle, S. L. 2010, *MNRAS*, 404, 458

Zhang, J., Luo, W., & Foucaud, S. 2015, *J. Cosmology Astropart. Phys.*, 1, 024

Zuntz, J., Kacprzak, T., Voigt, L., et al. 2013, *MNRAS*, 434, 1604

A. Probabilities for augmented moment noise

Section 2.5 describes a strategy of adding noise \mathbf{M}^A with covariance matrix \mathbf{C}_A to the moments \mathbf{M} of a selected target galaxy. We need to know the probability of selecting the galaxy and obtaining the total moments $\mathcal{M} = \mathbf{M} + \mathbf{M}_A$. Recall that the originally measured moments can also be expressed as $\mathbf{M} = \mathbf{M}^G + \mathbf{M}^n$, where the noise moments have known covariance matrix \mathbf{C}_M . We assume that both \mathbf{M}^n and \mathbf{M}^A are drawn from zero-mean multivariate Gaussians.

The galaxy is detected by the criterion $\mathbf{X} = \mathbf{X}^G + \mathbf{X}^n = 0$ and selected according to $f_1 < M_f < f_2$, and we will use the notation $\mathbf{M} \in S$ to denote when this condition is satisfied. We want the quantity

$$P(\mathcal{M}, s|G) = \mathcal{L}(\mathbf{X}^G) \int_{\mathbf{M} \in S} d\mathbf{M} |J(\mathbf{M})| P(\mathcal{M}, \mathbf{M}|G) \quad (\text{A1})$$

$$= \mathcal{L}(\mathbf{X}^G) \int_{(\mathbf{M}^n + \mathbf{M}^G) \in S} d\mathbf{M}^n (J^G + 2\mathbf{M}^G \cdot \mathbf{B} \cdot \mathbf{M}^n + \mathbf{M}^n \cdot \mathbf{B} \cdot \mathbf{M}^n) \mathcal{L}(\mathcal{M} - \mathbf{M}^G, \mathbf{M}^n). \quad (\text{A2})$$

Recall that we are approximating that the Jacobian derivative $J = |d\mathbf{X}/d\mathbf{x}_0| = \mathbf{M} \cdot \mathbf{B} \cdot \mathbf{M}$ is positive wherever the likelihood is non-negligible. Also note that in this Appendix we will suppress the dependence of moments and other quantities on the lensing \mathbf{g} and the displacement \mathbf{u} .

The joint distribution of the final and initial noise $\mathcal{L}(\mathcal{M} - \mathbf{M}^G, \mathbf{M}^n)$ is a zero-mean normal distribution. The covariance matrix of the concatenated noise vectors is known and fully specifies the distribution:

$$\mathbf{Cov}(\mathcal{M}) = \mathbf{C}_A + \mathbf{C}_M \equiv \mathbf{C} \quad (\text{A3})$$

$$\mathbf{Cov}(\mathbf{M}) = \mathbf{C}_M \quad (\text{A4})$$

$$\mathbf{Cov}(\mathcal{M}, \mathbf{M}) = \mathbf{C}_M. \quad (\text{A5})$$

Equation (A2) can be integrated over the Gaussian distribution; the result is

$$P(\mathcal{M}, s|G) = \mathcal{L}(\mathbf{X}^G) \Delta^2 x |2\pi\mathbf{C}|^{-1/2} \exp \left[-\frac{1}{2} (\mathcal{M} - \mathbf{M}^G)^T \mathbf{C}^{-1} (\mathcal{M} - \mathbf{M}^G) \right] \quad (\text{A6})$$

$$\times \left\{ Y \left[J(\tilde{\mathbf{M}}) + \text{Tr}(\mathbf{B}\mathbf{C}_A\mathbf{C}^{-1}\mathbf{C}_M) \right] - 2Y' \mathbf{Z}^T \mathbf{B} \tilde{\mathbf{M}} + Y'' \mathbf{Z}^T \mathbf{B} \mathbf{Z} \right\},$$

$$\tilde{\mathbf{M}} \equiv \mathbf{C}_M \mathbf{C}^{-1} \mathcal{M} + \mathbf{C}_A \mathbf{C}^{-1} \mathbf{M}^G, \quad (\text{A7})$$

$$\mathbf{Z} \equiv \frac{1}{\sigma_f} \mathbf{C}_A \mathbf{C}^{-1} \mathbf{C}_{Mf}, \quad (\text{A8})$$

$$\sigma_f^2 \equiv (\mathbf{C}_A \mathbf{C}^{-1} \mathbf{C}_M)_{ff}. \quad (\text{A9})$$

Here \mathbf{C}_{Mf} is row f of the original moment covariance matrix. The bounded Gaussian integral over

f results in the terms

$$Y = Y(\nu_{\min}, \nu_{\max}) \equiv \int_{\nu_{\min}}^{\nu_{\max}} d\nu e^{-\nu^2/2}, \quad (\text{A10})$$

$$Y' \equiv \frac{\partial Y}{\partial u_{\max}} - \frac{\partial Y}{\partial u_{\min}}, \quad (\text{A11})$$

$$Y'' \equiv \frac{\partial^2 Y}{\partial u_{\max}^2} - \frac{\partial^2 Y}{\partial u_{\min}^2}, \quad (\text{A12})$$

$$\nu_{\min} = \frac{1}{\sigma_f} \left(f_{\min} - \tilde{M}_f \right), \quad (\text{A13})$$

$$\nu_{\max} = \frac{1}{\sigma_f} \left(f_{\max} - \tilde{M}_f \right). \quad (\text{A14})$$

We replace Equation (38) with a weighted sum of (A6) over template galaxies G and their potential displacements \mathbf{x}_G . As before, derivatives with respect to \mathbf{g} propagate through the expressions into derivatives of the template moments. The total selection probability from Equation (40) is unaltered, since \mathbf{M}^A is not added to the moments until the selection process is complete.

B. Probabilities with translation-invariant noise vector

In some of our validation tests, we create moment vectors \mathbf{M} for targets by calculating \mathbf{M}^G directly from analytic formulae rather than pixelated images, and adding moment noise \mathbf{M}^n drawn from its known distribution. These simulated targets differ from image-based simulations in that the moment noise realization is invariant under shift of the coordinate origin \mathbf{x}_0 . In this case the Jacobian $J = d\mathbf{X}/d\mathbf{x}_0$ has contributions only from the underlying galaxy, not from the noise. We therefore must alter our formulae in this case of translation-invariant moment noise realizations. Equations (38) and (40) are altered by substituting these equations for the moment probability and the total selection probability of each galaxy:

$$P(\mathbf{M}, s|G) = \mathcal{L}(\mathbf{X}^G) \Delta^2 x J(\mathbf{M}^G) \mathcal{L}(\mathbf{M} - \mathbf{M}^G) \quad (\text{B1})$$

$$P(s|G) = \mathcal{L}(\mathbf{X}^G) \Delta^2 x J(\mathbf{M}^G) Y, \quad (\text{B2})$$

where Y is defined in Equation (34), and we suppress dependence on \mathbf{g} and \mathbf{u} .

In the case where we have added noise to the moments after selection in order to better smooth the template samples, we replace the formula (A6) with the simpler

$$P(\mathcal{M}, s|G) = \mathcal{L}(\mathbf{X}^G) \Delta^2 x |2\pi\mathbf{C}|^{-1/2} \exp \left[-\frac{1}{2} (\mathcal{M} - \mathbf{M}^G)^T \mathbf{C}^{-1} (\mathcal{M} - \mathbf{M}^G) \right] J(\mathbf{M}^G). \quad (\text{B3})$$

C. Derivatives and transformations of the Fourier-domain moments

Implementation of the BFD method requires that we calculate the derivatives of the Fourier-domain moments of our template galaxies under lensing distortions. We summarize here the formulae for these derivatives in the case of shear. We give the formulae in the case where the observed template surface brightness $I(\mathbf{x})$ is a continuous function. The transition to finite sampled data is straightforward.

Our convention for the Fourier transform of the image is

$$\tilde{I}(\mathbf{k}) = \int d^2x I(\mathbf{x}) \exp(-i\mathbf{k} \cdot \mathbf{x}). \quad (\text{C1})$$

We are interested in the change in moments after the image undergoes an affine transformation

$$I'(\mathbf{x}) = I(\mathbf{A}^{-1}\mathbf{x} - \mathbf{x}_0) \quad (\text{C2})$$

Standard Fourier manipulations give

$$\tilde{I}'(\mathbf{k}) = |\mathbf{A}| e^{-i\mathbf{k}' \cdot \mathbf{x}_0} \tilde{I}(\mathbf{k}') \quad (\text{C3})$$

$$\mathbf{k}' \equiv \mathbf{A}^T \mathbf{k}. \quad (\text{C4})$$

We define a two-component shear $\mathbf{g} = (g_1, g_2)$ of a galaxy image with the flux-conserving transformation

$$\mathbf{A}^{-1} = \frac{1}{\sqrt{1-g^2}} \begin{pmatrix} 1-g_1 & -g_2 \\ -g_2 & 1+g_1 \end{pmatrix}. \quad (\text{C5})$$

Note the BFD method is agnostic about the definition of shear; this is simply the choice for our implementation.

It is convenient to adopt a complex notation at this point:

$$\begin{aligned} k &\equiv k_x + ik_y & \partial &\equiv \frac{1}{2} \left(\frac{\partial}{\partial g_1} - i \frac{\partial}{\partial g_2} \right) \\ g &\equiv g_1 + ig_2 & \bar{\partial} &\equiv \frac{1}{2} \left(\frac{\partial}{\partial g_1} + i \frac{\partial}{\partial g_2} \right) \end{aligned} \quad (\text{C6})$$

With this notation the action of shear $\mathbf{k} \rightarrow (\mathbf{A}^T)^{-1} \mathbf{k}$ becomes

$$k \rightarrow k' = (1 - g\bar{g})^{-1/2} (k - g\bar{k}). \quad (\text{C7})$$

The moments we are interested in can also be compactly expressed in complex notation as well:

$$M'_\alpha = \int d^2k \tilde{I}(k) W(k'\bar{k}') F_\alpha(k'), \quad (\text{C8})$$

with

$$\begin{aligned}
M_0 &= M_f & F_0 &= 1 \\
M_1 &= X_x + iX_y & F_1 &= ik \\
M_2 &= M_+ + iM_\times & F_2 &= k^2 \\
M_r & & F_r &= k\bar{k}.
\end{aligned} \tag{C9}$$

The shear derivative operators can be rewritten as

$$\nabla_g = \mathbf{v}\partial + \bar{\mathbf{v}}\bar{\partial} \quad \mathbf{v} \equiv \begin{pmatrix} 1 \\ i \end{pmatrix} \tag{C10}$$

$$\nabla_g \nabla_g = \mathbf{v}\mathbf{v}^T \partial^2 + \bar{\mathbf{v}}\bar{\mathbf{v}}^T \bar{\partial}^2 + 2\mathbf{I}_2 \partial \bar{\partial} \quad \mathbf{I}_2 \equiv \begin{pmatrix} 1 & 0 \\ 0 & 1 \end{pmatrix} \tag{C11}$$

Now the derivatives of the moments with respect to shear are obtained by applying these operators to the moment definition (C8) after substituting in the shear wavevector transformation (C7). For each moment, the derivatives can be expressed as

$$\nabla_g M_\alpha = \int d^2k \tilde{I}(k) [W(k\bar{k})A_\alpha(k) + W'(k\bar{k})B_\alpha(k)] \tag{C12}$$

$$\nabla_g \nabla_g M_\alpha = \int d^2k \tilde{I}(k) [W(k\bar{k})C_\alpha(k) + W'(k\bar{k})D_\alpha(k) + W''(k\bar{k})E_\alpha(k)]. \tag{C13}$$

Table 2 lists the functions A, B, C, D, E , and F that yield the moments and their derivatives under shear. All of the moments and their derivatives are simple weighted polynomial moments of the galaxy Fourier transform.

A translation of the galaxy by \mathbf{x}_0 adds a factor $e^{-i\mathbf{k}\cdot\mathbf{x}_0}$ to $\tilde{I}(\mathbf{k})$ in the integrand of all the moments (and their derivatives).

Table 2. Functional forms of the integrands for moments and their derivatives, as defined by Equations (C13). The derivatives of the moments under translation in x and y directions are found by adding factors of $i(k + \bar{k})/2$ and $(k - \bar{k})/2$ to the entries, respectively.

Moment	M_0	M_1	M_2	M_r
$F_\alpha =$	1	ik	k^2	$k\bar{k}$
$A_\alpha = \mathbf{v} \times$	0	$-i\bar{k}$	$-2k\bar{k}$	$-\bar{k}^2$
$+\bar{\mathbf{v}} \times$	0	0	0	$-k^2$
$B_\alpha = \mathbf{v} \times$	$-\bar{k}^2$	$-ik\bar{k}^2$	$-k^2\bar{k}^2$	$-k\bar{k}^3$
$+\bar{\mathbf{v}} \times$	$-k^2$	$-ik^3$	$-k^4$	$-k^3\bar{k}$
$C_\alpha = \mathbf{I}_2 \times$	0	ik	$2k^2$	$4k\bar{k}$
$+\mathbf{v}\mathbf{v}^T \times$	0	0	$2\bar{k}^2$	0
$D_\alpha = \mathbf{I}_2 \times$	$4k\bar{k}$	$6ik^2\bar{k}$	$8k^3\bar{k}$	$8k^2\bar{k}^2$
$+\mathbf{v}\mathbf{v}^T \times$	0	$2i\bar{k}^3$	$4k\bar{k}^3$	$2\bar{k}^4$
$+\bar{\mathbf{v}}\bar{\mathbf{v}}^T \times$	0	0	0	$2k^4$
$E_\alpha = \mathbf{I}_2 \times$	$2k^2\bar{k}^2$	$2ik^3\bar{k}^2$	$2k^4\bar{k}^2$	$2k^3\bar{k}^3$
$+\mathbf{v}\mathbf{v}^T \times$	\bar{k}^4	$ik\bar{k}^4$	$k^2\bar{k}^4$	$k\bar{k}^5$
$+\bar{\mathbf{v}}\bar{\mathbf{v}}^T \times$	k^4	ik^5	k^6	$k^5\bar{k}$